THE EFFECT OF AUSTENITIZING TEMPERATURE UPON THE MICROSTRUCTURE AND MECHANICAL PROPERTIES OF EXPERIMENTAL Fe/Cr/C STEELS

Mark Carlson
(M. S. thesis)

March 1978

Prepared for the U. S. Department of Energy
under Contract W-7405-ENG-48

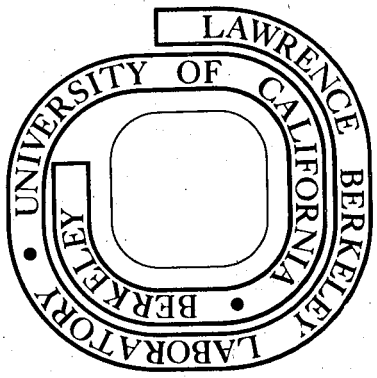

This report was done with support from the Department of Energy. Any conclusions or opinions expressed in this report represent solely those of the author(s) and not necessarily those of The Regents of the University of California, the Lawrence Berkeley Laboratory or the Department of Energy.

THE EFFECT OF AUSTENITIZING TEMPERATURE UPON THE MICROSTRUCTURE AND MECHANICAL PROPERTIES OF EXPERIMENTAL Fe/Cr/C STEELS

Contents

THE EFFECT OF AUSTENITIZING TEMPERATURE UPON THE MICROSTRUCTURE AND MECHANICAL PROPERTIES OF EXPERIMENTAL Fe/Cr/C STEELS

Mark Carlson

Materials and Molecular Research Division
Lawrence Berkeley Laboratory
and
Department of Materials Science and Mineral Engineering
University of California
Berkeley, California 94720

ABSTRACT

Increasing the austenitizing temperature from 870°C to 1100°C and higher can increase the fracture toughness, K_{Ic}, of common high strength structural steels from 50 to 100% with no loss in strength. However, the ductility (% reductionin area from a tensile test) decreases by as much as a factor of 3, and the Charpy impact energy either decreases or remains constant. The trend of increasing fracture toughness and decreasing Charpy impact energy appears to be inconsistent, but has been rationalized by considering the interaction of the stress field as a function of notch root radius and the microstructure.

The present study investigates the as-quenched strength and toughness of simple Fe/Cr/C alloys with an without titanium as a function of austenitizing temperature. For the ternary Fe/Cr/C alloys the results are consistent with earlier investigations, but the fracture toughness does not change with increasing austenitizing temperatures after 0.2 wt% Ti is added. The titanium forms carbides (TiC) that did not dissolve, providing a roughly constant number of crack nucleation sites, and preventing austenite grain growth up to 1100°C. The differences in

mechanical behavior, particularly the rounded notch toughness, are discussed and explained in terms of the microstructural characteristics of the alloys.

INTRODUCTION

In recent years it has been reported[1-11,25,36] that the fracture toughness, K_{Ic}, of low alloy high strength steels may be increased by as much as a factor of two with no loss in strength, by austenitizing at temperatures greater than 1100°C prior to quenching. The advantage of the increased toughness is to increase the critical flaw size (that causes unstable crack propagation) by a simple change in heat treatment. Although a corresponding increase in Charpy impact energy might be expected, results for 4340,[12,13] Fe/Cr/C,[9] En25,[14] 300M,[10] and a low carbon Cr-Ni-Mn[15] steel have shown either no increase or a decrease in impact energy, or an increase in transition temperature[15] for high austenitizing temperature in both the as-quenched and quenched and tempered (<350°C) conditions. Increases in impact energy (<50%) have been reported[16] for lower carbon 4330 and 4130 alloys.

One of the basic differences between the K_{Ic} and Charpy test is the radius of the notch at the root of the crack, i.e., $\rho \rightarrow 0$ mm for the K_{Ic} test and $\rho = 0.25$ mm for the Charpy test. By measuring the toughness of 4340 austenitized over the range 870°C to 1200°C as a function of the notch root radius, Ritchie and Horn[17] have shown that the conventionally austenitized (870°C) structure is tougher for root radii greater than 0.05 mm (0.002"), and the 1200°C structure tougher when $\rho < 0.05$ mm. The mode of failure for both was predominantly ductile rupture, but the 870°C structure showed evidence of quasicleavage and intergranular failure. For each structure the toughness is proportional to $\rho^{1/2}$ when ρ is greater than a critical radius ρ_o. Rice[41] and Ritchie and Horn[17] have proposed a model which predicts the $\rho^{1/2}$ dependence

for fibrous failure. If two structures have equal yield strengths, elastic moduli, and $\rho > \rho_o$ the tougher material will be the one which has the higher critical fracture strain, ε_f. Since $\rho \to 0$ for a fracture toughness test ($\rho < \rho_o$) the analysis by Rice is not valid for fracture toughness tests. For example a sample of 4340 austenitized at 1200°C and oil quenched has a greater fracture toughness, K_{Ic}, than one austenitized at 870°C, but a lower critical fracture strain. The value of ρ_o is characteristic of a given microstructure and is equal to the average spacing between those features in the microstructure that are responsible for initiating failure, e.g., inclusion or precipitate spacing for ductile fracture, and grain size for cleavage failure. A specimen with a very coarse microstructure, ρ_o large, will exhibit a high fracture toughness because of the additional amount of energy required to extend the plastic zone or raise the fracture stress over a larger distance necessary to initiate and ensure propagation of a crack.[12,13,15,17,19,20]

The purpose of the present investigation is to study the effect of austenitizing temperature upon three steels of similar composition, Fe-4 wt% Cr-0.35 wt% C, Fe-4 wt% Cr-0.30 wt% C, and Fe-4 wt% Cr-0.27 wt% C-0.2 wt% Ti. The 0.2% Ti alloy contains micron size titanium carbides tha do not dissolve and prevent grain growth up to an austenitizing temperature of 1100°C. The ternary Fe/Cr/C alloy contains sub-micron size chromium carbide that dissolve at 1000°C and do not prevent linear increases in grain size with austenitizing temperatures. The strength (Su,Sy), toughness (CVN, K_{Ic}), ductility (%RA), and an apparent fracture toughness, K_A, are measured, and the critical strain to failure calculated

using Ritchie and Horn's[18] theory. The microstructure is characterized at the optical and electron optical levels, and correlations are made between the mechanical properties and the observed microstructures.

The work is part of an ongoing program whose overall purpose is to determine the effects of composition and heat treatment upon the microstructure and mechanical properties of low alloy high strength structural steels.[9,21-28] The basic Fe/Cr/C alloy was selected by McMahon and Thomas[3,25] to offer good combinations of strength and toughness in both the as quenched and quenched and tempered conditions after austenitizing at temperatures higher than normal industrial practice (1100^{o}C vs 870^{o}C).

EXPERIMENTAL PROCEDURE

A. Material Preparation

The three alloys used in the investigation had the following compositions: alloy I Fe/4 wt% Cr/0.30 wt% C, referred to as the 0.3% C alloy, alloy II Fe/4 wt% Cr/0.35 wt% C, referred to as the 0.35% C alloy, and alloy III Fe/4 wt% Cr/0.27 wt% C/0.2 wt% Ti and will be referred to as the 0.2% Ti alloy. Alloys I and II were made at the Lawrence Berkeley Laboratory from electrolytically pure raw materials vacuum induction melted into 20 lb ingots and subsequently rolled or forged into 1" plates. Alloy III, also vacuum induction melted from electrolytically pure raw materials, was supplied courtesy Daido Steel Company of Japan in the form of 1" plate. All of the alloys were sandblasted to remove the oxide scale and homogenized at 1200^{o}C for 24 hours in vacuo before furnace cooling. The alloys were then hot rolled at 1100^{o}C down to 3/4" or 5/8" plates and then furnace cooled, resulting in a microstructure of coarse ferrite and pearlite.

B. Heat Treatment

Specimens were cut from the plate stock and rough machined to oversized dimensions before being austenitized in a vertical tube furnace filled with a positive pressure of argon gas to minimize decarburization. Austenitizing temperatures of 1290^{o}C, 1200^{o}C, 1100^{o}C, 1000^{o}C, and 870^{o}C were used and will be referred to as the 1290^{o}C structure, 1200^{o}C structure, 1100^{o}C structure, 1000^{o}C structure, and 870^{o}C structure respectively. The specimens were quenched into agitated oil at room temperature after solution treatment, and subsequently

ground to final dimensions under flood cooling to remove the decarburized layer.

C. Mechanical Testing

Tensile Testing

Standard ASTM tensile bars of 0.250" dia gage section 1.25" in length as shown in Fig. 1A were used to determine the strength, and ductility at room temperature ($22^{o}C$). A crosshead speed of 0.04 in./min was utilized in a 300 kip capacity MTS hydraulic testing machine. The orientation of the mechanical test specimens with respect to the rolling direction is shown in Fig. 2.

Fracture Toughness Testing

Compact tension specimens of dimensions shown in Fig. 1B were tested according to ASTM STP E399-74. The thickness, B, of the specimens was greater than $2.5(K_Q/\sigma_{ys})^2$ for all alloys and heat treatments investigated. Fatigue precracking and final testing was performed in the hydraulic MTS testing machine mentioned above.

Charpy Impact Testing

After heat treatment the Charpy specimens were ground under flood cooling to the dimensions shown in Fig. 1C. Testing was carried out in a Sonntag Universal Impact Machine of 0-60 ft-lbs capacity. A minimum of three specimens were tested for the basic Fe/Cr/C alloys, but there was only enough material available of the 0.2% Ti alloy to test one specimen for each heat treatment.

Error bars are shown in the graphed results when more than one specimen was tested and represent minimum 75% confidence limits. With

the exception of mechanical tests performed on Charpy bars two specimens were tested for each heat treatment for each alloy.

D. Metallography

Optical

Specimens for optical examination were cut from broken Charpy or fracture toughness specimens, mounted in Bakelite or Koldmount, and ground on 120 grit and 240 grit belt sanders under flood cooling to remove the deformed and heat affected zone from the cutting procedure. Final grinding was performed by hand on successively finer (240 grit, 320 grit, 400 grit and 600 grit) silicon carbide papers under flood cooling. Polishing was performed on 6 m and 1 m diamond paste wheels, and final polishing with a 0.05 m Al_2O_3 and H_2O slurry on a microcloth. A 5% Nital solution was used to reveal the microstructure, and a saturated solution of picric acid and dodecyclbenzene sulfonate in H_2O revealed the prior austenite grain boundaries.

Electron Microscopy

Single stage carbon extraction replicas were made from the etched optical metallographic specimens in order to determine the size, number, and type of submicron particles. Several hundred angstroms of carbon were deposited on the specimens in vacuo, and scored with a razor blade in to 2 mm x 2 mm squares. A solution of 10% Perchloric Acid in CH_3COOH at a potential of 20 volts was used to electrochemically remove the carbon film carrying the extracted carbides. The films were then transferred individually into successively more dilute solutions (50%, 20%, 10%, 0%) of CH_3COOH in H_2O before being fished out onto 200 mesh copper grids and dried on filter paper. A Siemens 1A electron

microscope operated at 100 kV was used to examine the specimens. The types of particles present was determined by analyzing the diffraction patterns.

Specimens for thin foils were obtained from 0.020" thick slices cut from Charpy or fracture toughness samples with an 0.008" thick abrasive wheel under flood cooling. Prior to spark cutting into discs of the appropriate size the slices were chemically thinned to 0.004" in a solution containing a few drops HF per 100 ml of H_2O_2. The discs were ground on 600 grit abrasive paper under flood cooling to a thickness of 0.0015" before electropolishing in a solution of 400 ml CH_3COOH, 75 gm CrO_3, and 21 ml H_2O at a potential of 20-35 volts. The foils were examined in either a Siemens 1A or Jem 7A electron microscope operated at 100 kV.

Fractography

For the purposes of protecting the fracture surface, replicating tape was softened in acetone and applied to the surface before the sample was cut away from the bulk specimen. Prior to observation the tape was removed and the specimen cleaned ultrasonically in acetone. The fracture surfaces were examined in either a JSM-V3 operated at 25 kV, or an AMR scanning electron microscope equipped with an EDAX x-ray detection system operated at 20 kV.

RESULTS

A. Microstructure

The microstructure of all three alloys for all heat treatments was auto-tempered dislocated lath martensite as described by Das and Thomas[21] and Thomas,[28] Figs. 15-24. The primary difference between the titanium and nontitanium steels was the carbide morphology. Optical micrographs of the 0.35% C and 0.30% carbon alloys as shown in Figs. 15, and for the 0.2% Ti alloy, Figs. 16 and 17. The average spacing between carbides for the 0.2% Ti alloy increased from 12 μm for the lowest to 20 μm for the highest austenitizing temperature. The average carbide size and the size distribution remained constant at ~1.5 μm and 0.5μm to 5 μm respectively. A reduction in the number of carbides between 0.5μm and 1.5μm in size accounts for the increase in average spacing with increasing austenitizing temperatures. A few widely spaced inclusions containing S, Mg, Al, Ca, and occasionally P were found in all of the alloys. Composition of the inclusions and large (~2 μm) carbides (except oxygen and carbon) was determined by means of energy dispersive analysis of x-rays. In the basic Fe/Cr/C alloy the inclusions contained between 10% and 80% Fe, and for the 0.2% Ti alloy the inclusions contained Ti instead of Fe. Small amounts of Cr (<5%) were found in all of the inclusions and in the carbides of the 0.2% Ti alloy. According to Freeman,[29] for an alloy containing Fe/0.2 wt% Ti/0.27 wt% C, all of the TiC would be dissolved when equilibrium was attained at 1200°C. What effect the addition of 4% Cr and the above impurities have on the stability of TiC in the steels under investigation is not known. Freeman also observed that Ostwald

ripening of undissolved TiC would be negligible, a result consistent with the data quoted earlier.

The submicron carbide size and spacing was determined at the electron optical level by means of carbon extraction replicas. Analysis of diffraction patterns revealed that they were predominantly Cr_7C_3, but $Cr_{23}C_6$ was also observed. According to Jackson[30] and Wada, et al.[31] all of the carbides would be dissolved at equilibrium for the compositions and temperatures involved in the present investigation. For the basic Fe/Cr/C alloys the carbides present in the 870°C structure were roughly 0.1 μm in diameter and inhomogeneously distributed, Fig. 18. The average spacing between the carbides was about 3 μm to 4 μm. The same carbides were also present in the 0.2% Ti alloy, but were not as large (<0.1 μm) and at roughly double the average spacing for the basic alloy. Increasing the austenitizing temperature to 1000°C reduced the average size by 25% to 50% and doubled the average spacing. Further increases in austenitizing temperatures resulted in very few undissolved chromium carbides.

The variation in lath, packet, and grain size is shown in Table 1, and the grain sizes plotted in Figs. 3 and 4. The lath width was independent of both composition and austenitizing temperature. Naylor and Blondeau observed that the lath width was dependent upon the cooling rate, decreasing and increasing cooling rates, and independent of austenitizing temperature for similar alloy compositions. The morphology and crystallography of lath martensites has been recently discussed by Thomas and Rao.[40] Grain size increased linearly with austenitizing temperature for the basic Fe/Cr/C alloy and remained

roughly constant at 20 μm for the 0.2% Ti alloy up to 1100°C and then increased linearly to 185 μm for the 1290°C treatment. The packet size followed the same trends as the grain size for a given alloy.

The presence of retained austenite between the martensite laths was observed for all alloys and austenitizing temperatures. Analysis of selected area diffraction patterns revealed that the orientation relationship between the austenite and marten site was the K-S relationship,[32] i.e.,

$$(111)_{\alpha},//(110)_{\gamma}$$
$$(211)_{\alpha},//(21\bar{1})_{\gamma} \quad .$$

Thomas and Rao[40] have observed both the Kurdjumov-Sachs and the Nishiyama-Wasserman orientation relationships in the same packet, but for these alloys the K-S relation is the dominant one. By means of dark field imaging of retained austenite spots in the diffraction pattern the morphology was determined, Figs. 19-21. For the 0.2% Ti alloy austenitized at all temperatures and the 870°C structure of the base alloy the films were not continuous around the martensite laths, Figs. 19,20. Increasing the austenitizing temperature to 1000°C and higher resulted in nearly continuous films of austenite around the individual laths, Fig. 21, for the 0.35%C and 0.3%C alloys.

The relatively high M_s temperature (M_s ~ 350°C, M_f ~ 250°C) combined with the cooling rate for an agitated oil quench resulted in autotempered carbides being present in all of the thin foils observed. Examples are shown in Figs. 22 and 23. Analysis of the diffraction pattern combined with dark field imaging revealed that the carbides were Fe_3C and followed the Bagaryatskii orientation relationship,[33]

$$(100)_{Fe_3C}//(0\bar{1}1)_{\alpha}$$
$$(010)_{Fe_3C}//(1\bar{1}\bar{1})_{\alpha}$$
$$(001)_{Fe_3C}//(211)_{\alpha}.$$

The carbides were rod shaped and roughly 700Å in length and 200Å in diameter.

Small amounts of transformation twinning (<1%) was observed in all of the alloys. Examples are shown in Figs. 24 and 21 of the 0.35% C alloy austenitized at 1200°C. For the 0.2% Ti alloy twinning was less frequently observed compared to the basic alloy. The probability of observing twinning increased with austenitizing temperature, as expected for higher amounts of carbon in solution.

B. Mechanical Properties

The room temperature mechanical properties (22°C) for the three alloys are graphed in Figs. 5-14. For the Fe/Cr/C alloys the results are consistent with those of previous investigators,[1-11] i.e., yield and ultimate strength fairly constant, Fig. 5, and the fracture toughness increasing with the austenitizing temperature up to 1100°C, Fig. 6. Charpy impact energy, Cv, decreased slightly from 22 J at 870°C to 16 J for the 0.3% C alloy and varied between 18 J and 23 J for the 0.35% C alloy, Fig. 7. The roughly constant strengths may be the result of a balance between the increased packet and grain size which decreases the strength and the increased amount of solute (esp. carbon) in solution, increasing the strength, when the austenitizing temperature is increased. If there is a continuous film of austenite surrounding the individual laths continuous slip planes between the laths would not be expected.

The laths may therefore act like very small subgrains whose size remains constant with increasing austenitizing temperature.

The increase in toughness is associated with the following changes in the mode of failure (characteristic of both the fracture toughness and Charpy specimens): i) 870°C structure, quasicleavage and void coalescence, Fig. 25a; ii) 1000°C structure void coalescence with some quasicleavage, Fig. 25b; iii) 1100°C structure, void coalescence and small amounts of quasicleavage, Fig. 25c; and iv) 1200°C structure, intergranular microvoid coalescence (IMC), Fig. 25d and 26. Schulz and McMahon[34] have observed the same type of IMC failure in a series of 3.5% Ni/1.7 Cr steels which were slowly cooled from 1250°C to 900°C before quenching. They observed second phase particles with high concentrations of Cr and S along the prior austenite grain boundaries, presumably CrS. The same alloy oil quenched from 1250°C failed in a transgranular manner. Their data indicate that the CrS dissolves somewhere between 900°C and 1250°C and then reprecipitated out on the austenite grain boundaries when held at 900°C prior to quenching. Prior austenite grain boundaries of the fractured K_{Ic} specimens (1200°C treatment) were inspected at high magnification (10,000x), but no second phase particles were observed. The agitated oil quench was fast enough to supress precipitation, but segregation may have occurred, weakening the boundaries relative to the matrix, causing this intergranular type failure. A reduction in fracture toughness usually accompanies the impurity segregation and precipitation at grain boundaries after austenitizing at high temperatures and is usually referred to as "overheating."[34,35]

Youngblood and Raghavan[10] have also observed a change in the mode of failure from quasicleavage to void coalesence for 300 M steel when the austenitizing temperature was increased from 871°C to 982°C. They coated the fracture surface of one of the 871°C structures with a thin layer of gold and observed the fracture surface at high magnification. Particles whose dimensions were on the order of the undissolved particles present in the 871°C structure were concentrated only in the quasicleavage portions of the fractographs.[10] Chipperfield and Knott[20] have suggested that the presence of submicron particles reduce toughness by effectively decreasing the value of the local strain necessary to promote failure.[20]

The yield and ultimate strengths for the 0.2% Ti alloy followed the same trends, but did not remain constant when the austenitizing temperature was increased, Fig. 8. As shown in Table 1, the second phase particle spacing, lath, packet, and grain size are roughly the same for the 870°C and 1000°C structures. The increase in strength for the 1000°C structure compared to the 870°C structure is probably due to the increased carbon in solution when most of the submicron chromium carbides dissolve at 1000°C. Increasing the austenitizing temperature to 1100°C causes a decrease in strength which can not be readily explained. The 1000°C and 1100°C structures have roughly the same lath, packet, grain, and second phase particle spacing. The decrease in particle spacing is within experimental error (5%) and would not be expected unless the composition of the particles was changing. Because of the wide variation in composition of the particles due to the presence of impurities and the size of the particles ~1 μm in relation to the spatial resolution 1-2 μm

of the energy dispersive x-ray analysis instrument an extensive analysis of the composition of the particles was not attempted. The volume fraction of the carbides (<1%) was not sufficient to yield any recognizable peaks in an x-ray diffractometer trace.

Further increases in the austenitizing temperature to 1200°C and 1290°C resulted in increasing strengths, packet and prior austenite grain sizes. The observed dissolution of the smaller particles (~1 μm) increasing the amount of solute in solution, more than offsetting the decrease in strength expected with larger grain size.

In constrast to the basic Fe/Cr/C alloys the 0.2% Ti alloy did not exhibit any significant change in fracture toughness, K_{Ic}, when the austenitizing temperature was increased from 870°C to 1290°C, Fig. 9. Parker and Zackay[36] have also reported no change in fracture toughness, K_{Ic}, when the austenitizing temperature was increased from 870°C to 1200°C for a pair of Fe-1 Mo-0.34 C, Fe-1 Mo-0.35 C-3 Ni steels. Subsequent microstructural analysis revealed no undissolved carbides present in any of the microstructures.[4]

Examination of the fracture surfaces revealed that the mode of failure for all of the heat treatments was predominantly quasicleavage with some microvoid coalescence for both the fracture toughness and Charpy tests, Figs. 27a-d. An increase in the amount of void coalescence was observed at the fatigue/fracture interface. Particles high in Ti were observed at the bottom of some of the dimples, and occasionally what looks like large particles fractured into several pieces were also observed, Fig. 28. Second phase particles were observed

in the quasicleavage regions of the fracture surface, but in numbers small compared to the average carbide spacing.

Charpy impact energy for the 0.2% Ti alloy varied between 15 J and 20 J, except for the 1000°C structure (25 J),[20] Fig. 10. The crack initiated by dimpled rupture mechanisms in a region 0.1 mm to 0.2 mm wide (5 to 10 times the average particle spacing) at the root of the notch and propagated through the specimen leaving a fracture surface characteristic of quasicleavage for all heat treatments, Fig. 29.

The ductility (as measured by percent reduction in area for a tensile specimen) decreases when the austenitizing temperature is increased from 870°C to 1100°C and higher for all three alloys. The reduction in ductility amounts to a factor of 3 for the 0.35% C alloy, 2.4 for the 0.30% C alloy and roughly 1.4 for the low carbon titanium alloy, Figs. 11 and 12. The actual amount of carbon in solution for the 0.2% Ti alloy is less than the nominal 0.27% because of the titanium carbides. This trend of decreasing ductility with increasing austenitizing temperatures is common to many of the alloys investigated by previous authors.[4,6,12,13]

DISCUSSION

Despite the significant improvements in fracture toughness observed for a variety of structured steels, 4340,[12,13] 4330,[16] 300-M[3,10] En 25,[14] 4130,[16] 0.4 C-5 Mo,[36] 0.3 C-5 Mo,[36] when the austenitizing temperature is increased to 1100°C or 1200°C similar increases in Charpy impact energy are not reported.[9,10,12-15] Ritchie, et al.[12,13] and Ritchie and Horn[17] have suggested that this apparent inconsistency can be explained by comparing the relative toughness of specimens austenitized at conventional (870°C) temperature vs higher austenitizing treatments as a function of notch root radius. Models which account for the effect of notch acuity on toughness have been proposed by Ritchie, et al.[12] (stress controlled failure) based on the work by Tetelman, et al.[19] for cleavage failure of mild steel, and by Rice[41] and Ritchie and Horn[17] (strain controlled failure) based on the work by Rice,[18] for a constant strain to failure, ε_f, at the notch root.

After Ritchie, et al.[12]

$$K_A \approx 2.9\ \sigma_y \left[\exp\left(\frac{\sigma_f}{\sigma_y} - 1\right) - 1\right]^{1/2} \rho^{1/2} \quad , \qquad (1)$$

After Ritchie and Horn[18]

$$K_A \approx \left(\frac{3}{2}\ \sigma_y E \varepsilon_f\right)^{1/2} \rho^{1/2} \quad , \qquad (2)$$

where K_A is the apparent fracture toughness, σ_f is the fracture stress, σ_y the yield stress, E the modulus of elasticity, ε_f is the critical strain to failure, and ρ the notch root radius.

For a given structure the toughness is proportional to the square root of the root radius and is independent of the type of failure

(stress or strain controlled). Experimental results verify the $\rho^{1/2}$ dependence,[12,13,37,20,17] and Ritchie, et al.[12,13] and Ritchie and Horn[17] have shown that this is independent of strain rate and shear lip effects for 4340. When the radius of the notch is decreased below a critical value, ρ_o (characteristic of a given structure), the toughness is constant. The value of ρ_o has been found to vary numerically with the interparticle spacing for low strength steels studied by Chipperfield and Knott,[20] and the grain size[12] in the work by Ritchie, et al.[12] The argument put forward to account for the existence of a limiting root radius is that the stress[19,12] or strain[20,17,37] at the crack tip must be exceeded over a distance greater than the microstructural feature which initiates failure, e.g., the plastic zone size must exceed the interparticle spacing for fibrous rupture because decohesion or fracture of the particle (carbide) initiates failure.

A series of Charpy sized specimens of the two low carbon alloys (0.3% C and 0.2% Ti) were machined with 0.30 mm (0.012") R notches. The specimens were loaded to failure in three point bend and the toughness calculated at maximum load,[12,38] Fig. 13. All specimens failed after little or no measurable ductility occurred. A trend of decreasing toughness, K_A, with increasing austenitizing temperature is evident for both alloys and roughly follows the shapes of the % reduction in area curves, Figs. 10 and 11.

By assuming that failure for the 0.3% C and 0.2% Ti alloys is strain controlled the critical strain to failure can be calculated using Equation (2) and is shown in Fig. 14. The critical fracture strain decreases continuously for the 0.30% C alloy, and for

austenitizing temperature greater than 1100°C the fracture strain for the 0.2% Ti alloy also decreases, i.e., the critical strain to failure decreases with increasing prior austenite grain size. The increase in fracture strain, ε_f, for the 1100°C structure compared to the 870°C structure for the 0.2% Ti alloy is coincident with a decrease in the number of strain inhibiting submicron particles.[20]

Clausing,[39] Ritchie and Horn,[17] and Hahn, et al.[37] have shown that the critical strain to failure calculated from data obtained in toughness tests is equal to Refs. 37,39 or follows the same trends[17] as the plane strain ductility[17,39] or the strain at failure for the outer fiber of a bend specimen.[37]

CONCLUSIONS

The microstructure and room temperature mechanical properties of three chemically similar low alloy high strength steels has been studied after austenitizing over a range of temperatures between 870°C and 1300°C.

i) The fracture toughness, K_{Ic}, does not increase with austenitizing temperature if the microstructure does not coarsen, i.e., the characteristic distance ρ_o does not significantly increase.

ii) The apparent toughness of low alloy high strength steels in the presence of a notch whose radius, ρ, is greater than the characteristic distance decreases with increasing prior austenite grain sizes and increases with decreasing numbers of submicron particles (carbides or inclusions).

iii) Due to the lack of significant changes in the morphology of the retained austenite no statements can be made concerning this effect of retained austenite upon the toughness of the steels used in this investigation.

ACKNOWLEDGEMENTS

The author would like to express his gratitude to Professor Gareth Thomas for his support, patience, and guidance during the course of the investigation. He would also like to thank Dr. B.V.N. Rao for many helpful discussions, review of the manuscript, and especially his friendship for the past few years.

The author wishes to thank Professors Iain Finnie and Earl Parker for their review of the manuscript.

Special thanks are extended to the technical support staff of the Materials and Molecular Research Division.

This work was supported by the United States Department of Energy through the Materials and Molecular Research Division of the Lawrence Berkeley Laboratory.

REFERENCES

1) V. F. Zackay, E. R. Parker, R. D. Goolsby, and W. E. Wood, Nature Phys. Sci. 236, 188 (1972).

2) G. Clark, R. O. Ritchie, and J. F. Knott, Nature Phys. Sci. 239, 104 (1972).

3) J. McMahon, M.S. Thesis, University of California, Lawrence Berkeley Laboratory Report, LBL-1181 (1973).

4) T. Thom, D. Eng. Thesis, University of California, Lawrence Berkeley Laboratory Report, LBL-1856 (1973).

5) R. O. Ritchie and J. F. Knott, Met. Trans. 5, 782 (1974).

6) G. Y. Lai, W. E. Wood, R. A. Clark, V. F. Zackay, and E. R. Parker, Met. Trans. 5, 1663 (1974).

7) W. E. Wood, Eng. Fract. Mech. 7, 219 (1975).

8) E. R. Parker and V. F. Zackay, Eng. Fract. Mech. 7, 371 (1975).

9) M. F. Carlson, B. V. N. Rao, R. O. Ritchie, and G. Thomas, Proc. 4th Intl. Conf. on the Strength of Metals and Alloys, (France), 2, 509 (1976).

10) J. L. Youngblood and M. Raghavan, Met. Trans. 8A, 1439 (1977).

11) D. S. McDarmaid, Metals Tech. 4, 7 (1978).

12) R. O. Ritchie, B. Francis, and W. L. Server, Met. Trans. 7A, 831 (1976).

13) R. O. Ritchie, B. Francis, and W. L. Server, Met. Trans. 8A, 1197 (1977).

14) W. G. Ferguson, N. E. Clark, and B. R. Watson, Metals Tech. 3, 208 (1976).

15) J. P. Naylor and R. Blondeau, Met. Trans. 7A, 891 (1976).

16) W. E. Wood, Met. Trans. 8A, 1195 (1977).

17) R. O. Ritchie and R. M. Horn, Met. Trans. 9A, 331 (1978).

18) J. R. Rice, J. Applied Mechanics, Trans. ASME Series E 35, 379 (1968).

19) A. S. Tetelman, T. R. Wilshaw, and C. A. Rau, Jr., Intl. J. Fract. Mechanics, 4 Nr2, 147 (1968).

20) C. G. Chipperfield and J. F. Knott, Metals Tech. 2, 45 (1975).

21) S. K. Das and G. Thomas, Trans. ASM 62, 659 (1969).

22) D. Huang and G. Thomas, Met. Trans. 2, 1587 (1971).

23) M. Raghavan and G. Thomas, Met. Trans. 2, 3433 (1971).

24) G. Thomas, Iron and Steel International 46, 451 (1973).

25) J. McMahon and G. Thomas, Proc. Int. Conf. Microstructure and Design of Alloys, (Cambridge), Inst. of Metals (London) 1, 180 (1973).

26) R. A. Clark and G. Thomas, Met. Trans. 6A, 969 (1975).

27) B. V. N. Rao and G. Thomas, Mat. Sci. and Eng. 20, 195 (1975).

28) G. Thomas, Met. Trans. 2, 2373 (1971).

29) S. Freeman, in Effect of Second Phase Particles on the Mechanical Properties of Steel, Proc. ISI (London), 152 (1971).

30) R. S. Jackson, JISI 193, 163 (1970).

31) T. Wada, H. Wada, J. F. Elliott, and J. Chipman, Met. Trans. 3, 2865 (1972).

32) G. V. Kurdjumov and G. Sachs, Z. Physik. 64, 325 (1930).

33) Y. A. Bagaryatskii, Dok. Akad. Nauk. SSSR 73, 1161 (1950).

34) B. J. Schulz and C. J. McMahon, Met. Trans. 4, 2485 (1973).

35) R. O. Ritchie and J. F. Knott, Met. Trans. 5, 782 (1974).

36) E. R. Parker and V. F. Zackay, Eng. Frach. Mech. 7, 371 (1975).

37) G. T. Han, R. G. Hoagland, and A. R. Rosenfield, Met. Trans. 7A, 49 (1976).

38) T. R. Wilshaw, C. A. Rau, and A. S. Tetelman, Eng. Fract. Mech. 1, 191 (1968).

39) D. P. Clausing, Int. J. Fract. Mech. 6, Nr1, 85 (1970).

40) G. Thomas and B. V. N. Rao, Int. Conf. on Martensite Transformation, Kiev USSR, LBL-6242, May 1977, in press.

41) J. R. Rice. Division Engineering Report E39, Brown University, Providence, RI, 1967.

Table I.

Austenitizing Temperature	Lath Width, m			Martensite Packet Size, m			Prior Austenite Grain Size, m			Average Second Phase Particle Spacing, 0.29 Ti (center to center), m
	0.35%C	0.3%C	0.2%Ti	.35C	.3C	.2Ti	.35C	.3C	.2Ti	
870°C	0.3	0.37	N/D	N/D	26	14	31	29	18	12
1000°C	0.47	0.35	0.39	N/D	31	16	90	111	22	13.9
1100°C	0.41	0.39	0.31	N/D	42	16	148	202	28	13.5
1200°C	0.38	0.39	0.29	N/D	47	28	179	254	120	14
1290°C	--	--	0.36	N/D		51	--	--	185	20

N/D - Not determined.

FIGURE CAPTIONS

Fig. 1. Sketches of mechanical test specimens (a) tensile (b) fracture toughness, K_{Ic}, and (c) Charpy V-notch.

Fig. 2. Schematic diagram showing orientations of mechanical test specimens with respect to the plate stock.

Fig. 3. Plot of prior austenite grain size versus austenitizing temperature for the 0.3% C and 0.35% C alloys.

Fig. 4. Plot of prior austenite grain size versus austenitizing temperature for the 0.2% Ti alloy.

Fig. 5. Plot of yield (Sy) and ultimate (Su) strengths versus austenitizing temperature for the 0.3% C and 0.35% C alloys.

Fig. 6. Plot of fracture toughness, K_{Ic}, versus austenitizing temperature for the 0.3% C and 0.35% C alloys.

Fig. 7. Plot of Charpy impact energy, Cv, versus austenitizing temperature for the 0.3% C and 0.35% C alloys.

Fig. 8. Plot of yield (Sy) and ultimate (Su) strengths versus austenitizing temperature for the 0.2% Ti alloy.

Fig. 9. Plot of fracture toughness, K_{Ic}, versus austenitizing temperature for the 0.2% Ti alloy.

Fig. 10. Plot of Charpy impact energy, Cv, versus austenitizing temperature for the 0.2% Ti alloy.

Fig. 11. Plot of percent reduction in area, % R_A, versus austenitizing temperature for the 0.3% C and 0.35% C alloys.

Fig. 12. Plot of percent reduction in area, % R_A, versus austenitizing temperature for the 0.2% Ti alloy.

Fig. 13. Plot of apparent fracture toughness, K_A, versus austenitizing temperature for the 0.3% C and 0.2% Ti alloys.

Fig. 14. Plot of critical strain to failure, ε_f, versus austenitizing temperature for the 0.3% C and 0.2% Ti alloys.

Fig. 15. Optical micrographs of the 0.35% C alloy austenitized at (a) 870°C, (b) 1000°C, (c) 1100°C, and (d) 1200°C.

Fig. 16. Optical micrographs of the 0.2% Ti alloy austenitized at (a) 870°C, (b) 1000°C, (c) 1100°C, (d) 1200°C, and (e) 1290°C.

Fig. 17. Optical micrographs of the 0.2% Ti alloy austenitized at (a) 870°C, (b) 1100°C, (c) 1200°C, and (d) 1290°C, unetched.

Fig. 18. Transmission electron micrographs of a 0.3% C alloy specimen austenitized at 870°C. Undissolved carbides in the bright field image reverse contrast in the dark field image, (a). Auto-tempered carbides (b) can also be seen in the dark field image.

Fig. 19. Transmission electron micrograph of a 0.35% C alloy specimen austenitized at 870°C. A bright and dard field pair showing the morphology of retained austenite. A $(200)_\gamma$ reflection was imaged to obtain the dark field image.

Fig. 20. Transmission electron micrograph of a 0.2% Ti alloy sample austenitized at 1290°C. The presence of retained austenite is determined by analysis of the diffraction pattern and dark field imaging. The $(002)_\gamma$ reflection was imaged to obtain the dark field micrograph.

Fig. 21. Transmission electron micrograph of a 0.35% C alloy sample austenitized at 1200°C. The difference in morphology of the retained austenite can be seen by comparing Figs. 19 and 20 with Fig. 21. Films of retained austenite are nearly continuous around the laths when the base alloy is austenitized at 1000°C or higher. Some twinning is also evident in the bright field image. The addition of titanium causes the films to be less continuous even when it is austenitized at higher temperatures.

Fig. 22. Transmission electron micrograph of a 0.35% C alloy sample austenitized at 1000°C. A bright field dark field pair showing auto-tempered Fe_3C.

Fig. 23. Transmission electron micrograph of a 0.2% Ti alloy sample austenitized at 1200°C. Auto-tempered iron carbides (Fe_3C) reverse contrast in (b and c) when the reflections shown are imaged.

Fig. 24. Transmission electron micrograph of a 0.35% C alloy specimen austenitized at 1200°C. Transformation twinning is shown by imaging the matrix and twin related reflections. An auto-tempered carbide reflection was unintentionally included in the objective aperture when the twin related spot was imaged.

Fig. 25. Scanning electron micrographs of fracture surfaces of fracture toughness specimens austenitized at (a) 870°C (0.35% C alloy) quasicleavage, (b) 1000°C (0.35% C alloy) void coalescence (c) 1100°C (0.3% C alloy) void coalescence, and (d) 1200°C (0.35% C alloy) intergranular microvoid coalescence.

Fig. 26. Lower magnification fractograph taken with SEM of 0.30% C alloy specimen austenitized at 1200°C.

Fig. 27. Fractographs of fracture toughness, K_{Ic}, specimens austenitized at (a) 870°C, (b) 1000°C, (c) 1100°C, and (d) 1200°C for the 0.2% Ti alloy. The failure was predominantly quasicleavage except for some dimpled rupture evident in the region of the "pop in."

Fig. 28. High magnification fractograph showing what is apparently fractured titanium carbides at the bottom of voids. Energy dispersive x-ray analysis revealed that the particles were primarily Ti with a little Cr. Since the detector cannot see carbon the particles are assumed to be TiC.

Fig. 29. Fractograph of a broken Charpy V-notch specimen showing a region of dimpled rupture near the base of the notch (top of page). The remainder of the sample failed by quasicleavage.

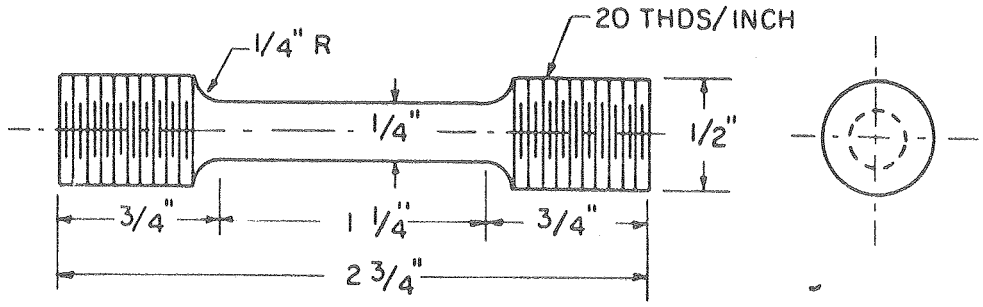

A. ROUND TENSILE SPECIMEN

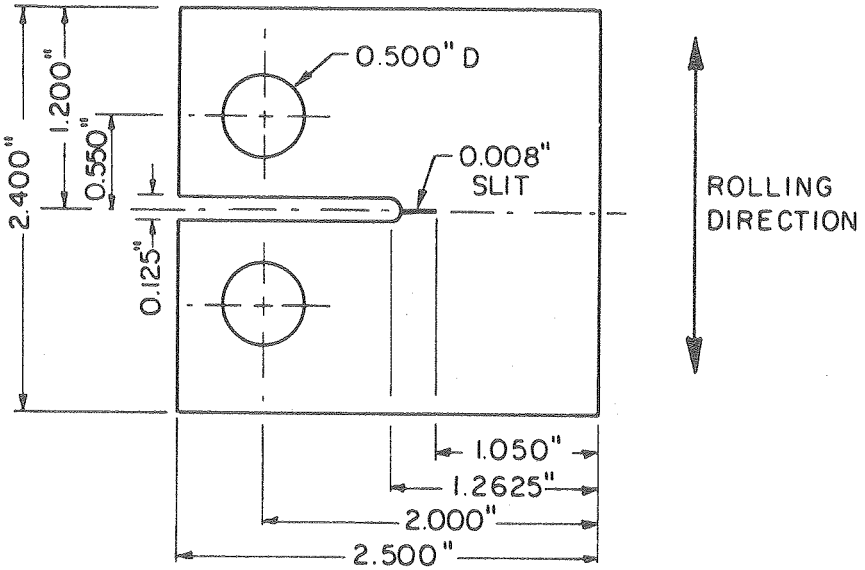

B. FRACTURE TOUGHNESS SPECIMEN

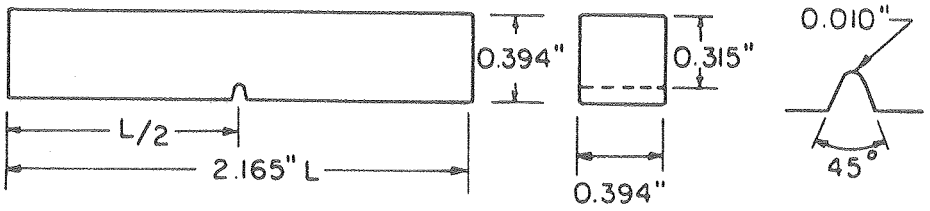

C. CHARPY V-NOTCH IMPACT SPECIMEN

XBL 754-6176

Fig. 1

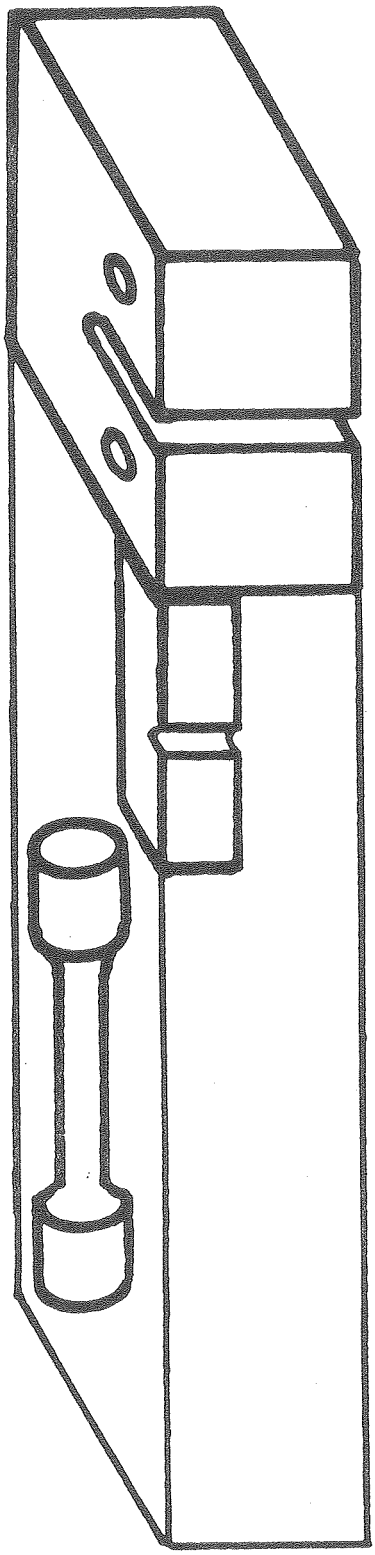

XBL 7612-10410B

Fig. 2

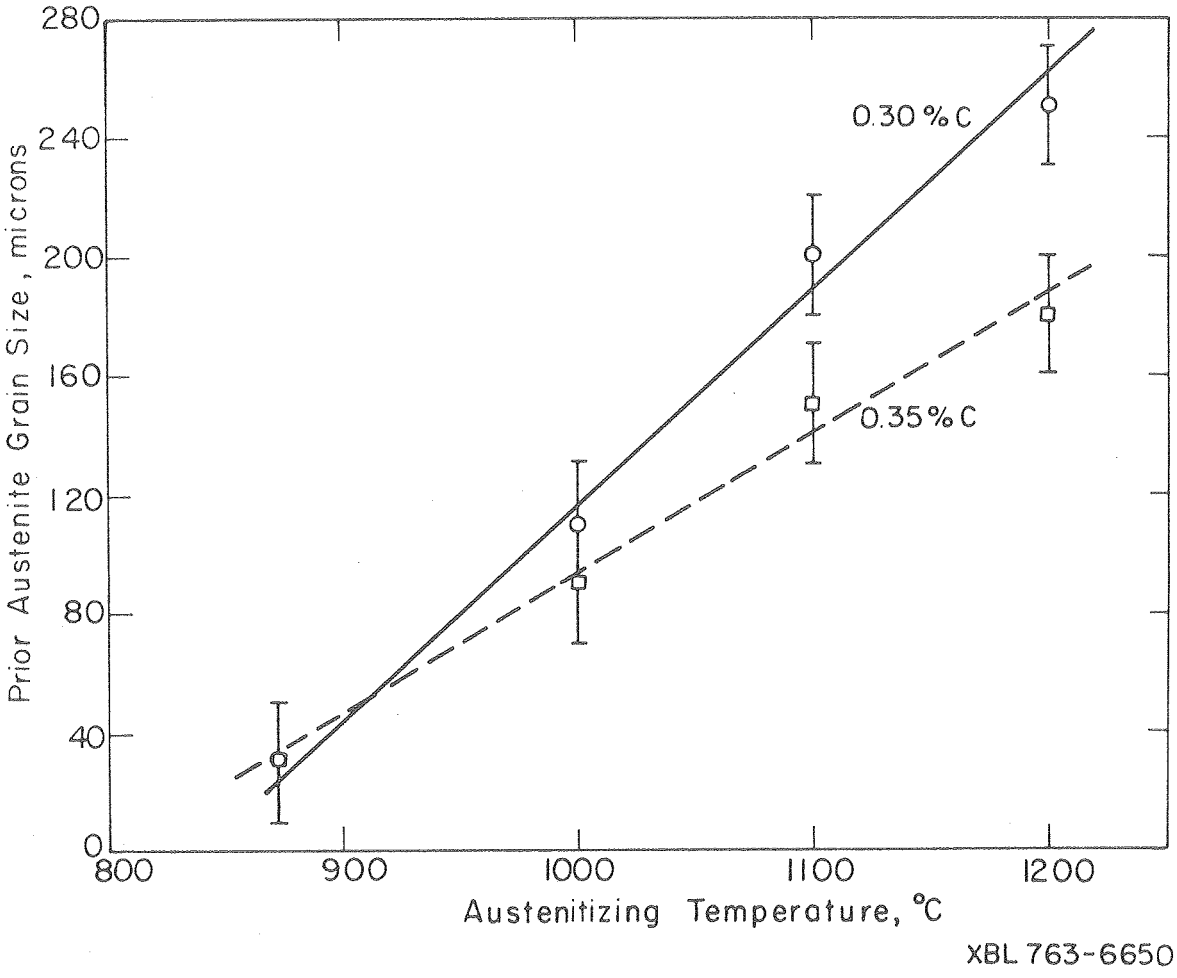
280
240
200
160
120
80
40
0
800
900
1000
1100
1200
Prior Austenite Grain Size, microns
Austenitizing Temperature, °C
0.30 % C
0.35 % C
XBL 763-6650

Fig. 3

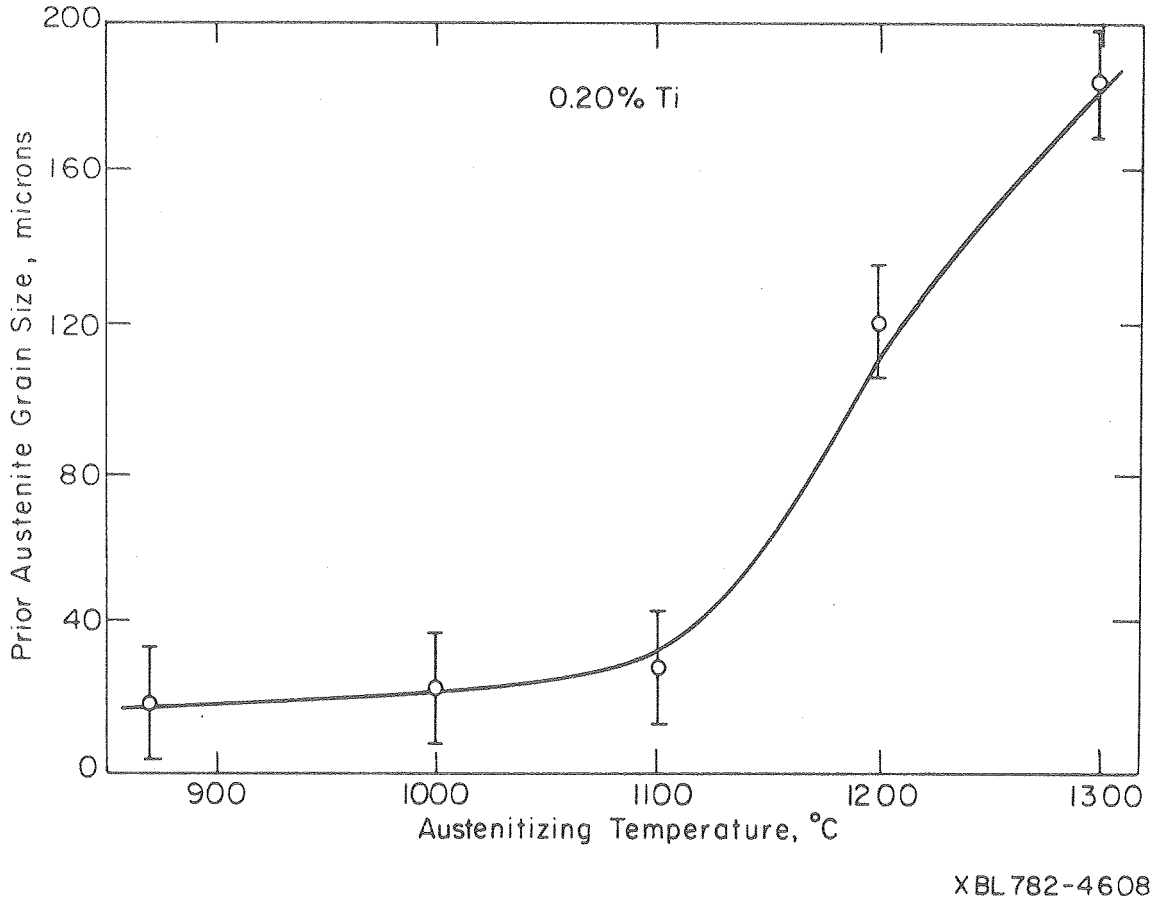
0.20% Ti
Prior Austenite Grain Size, microns
200
160
120
80
40
0
900
1000
1100
1200
1300
Austenitizing Temperature, °C
XBL 782-4608

Fig. 4

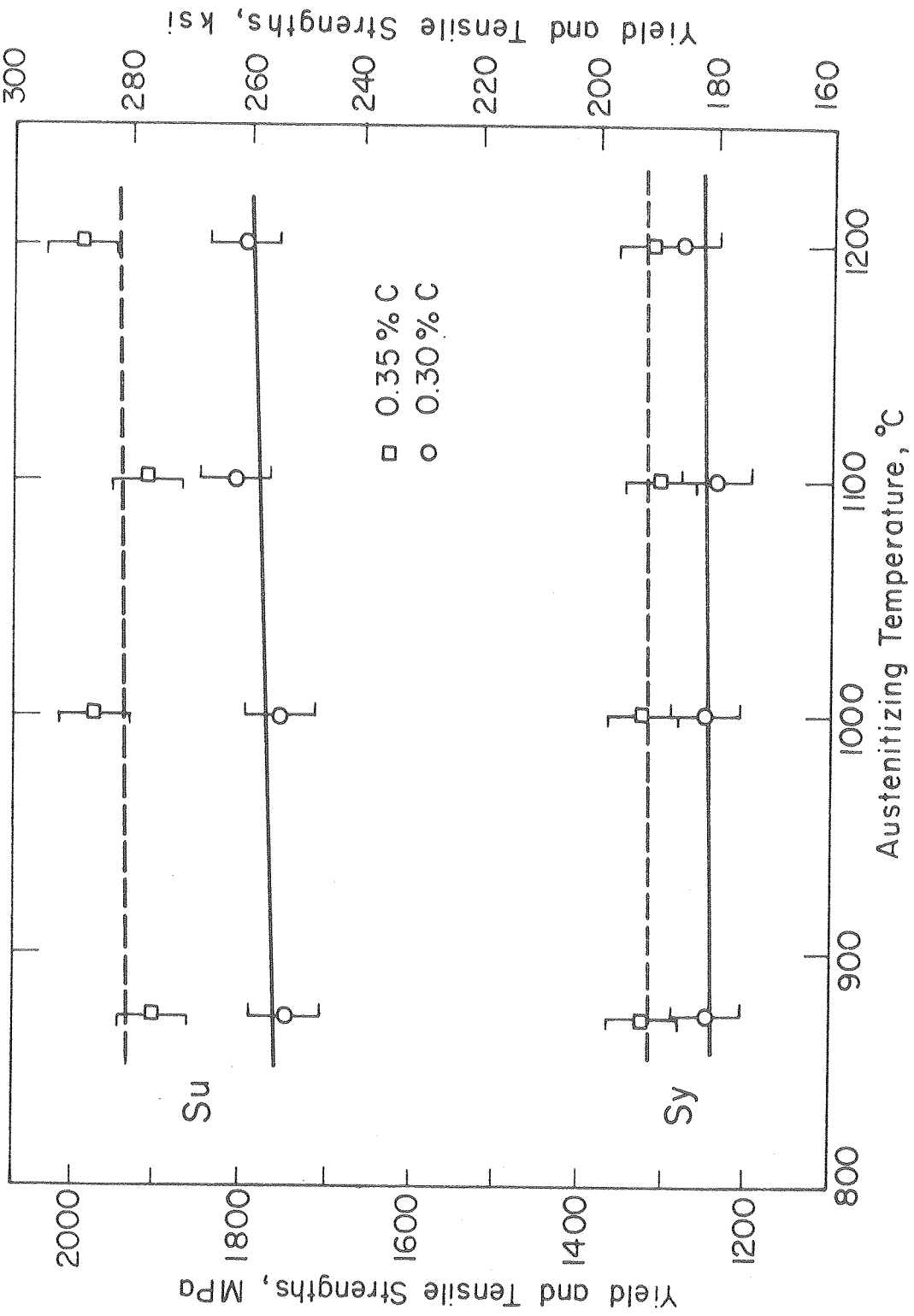
Yield and Tensile Strengths, MPa
2000
1800
1600
1400
1200
Yield and Tensile Strengths, ksi
300
280
260
240
220
200
180
160
800
900
1000
1100
1200
Austenitizing Temperature, °C
Su
Sy
0.35 % C
0.30 % C
XBL 762-6512A

Fig. 5

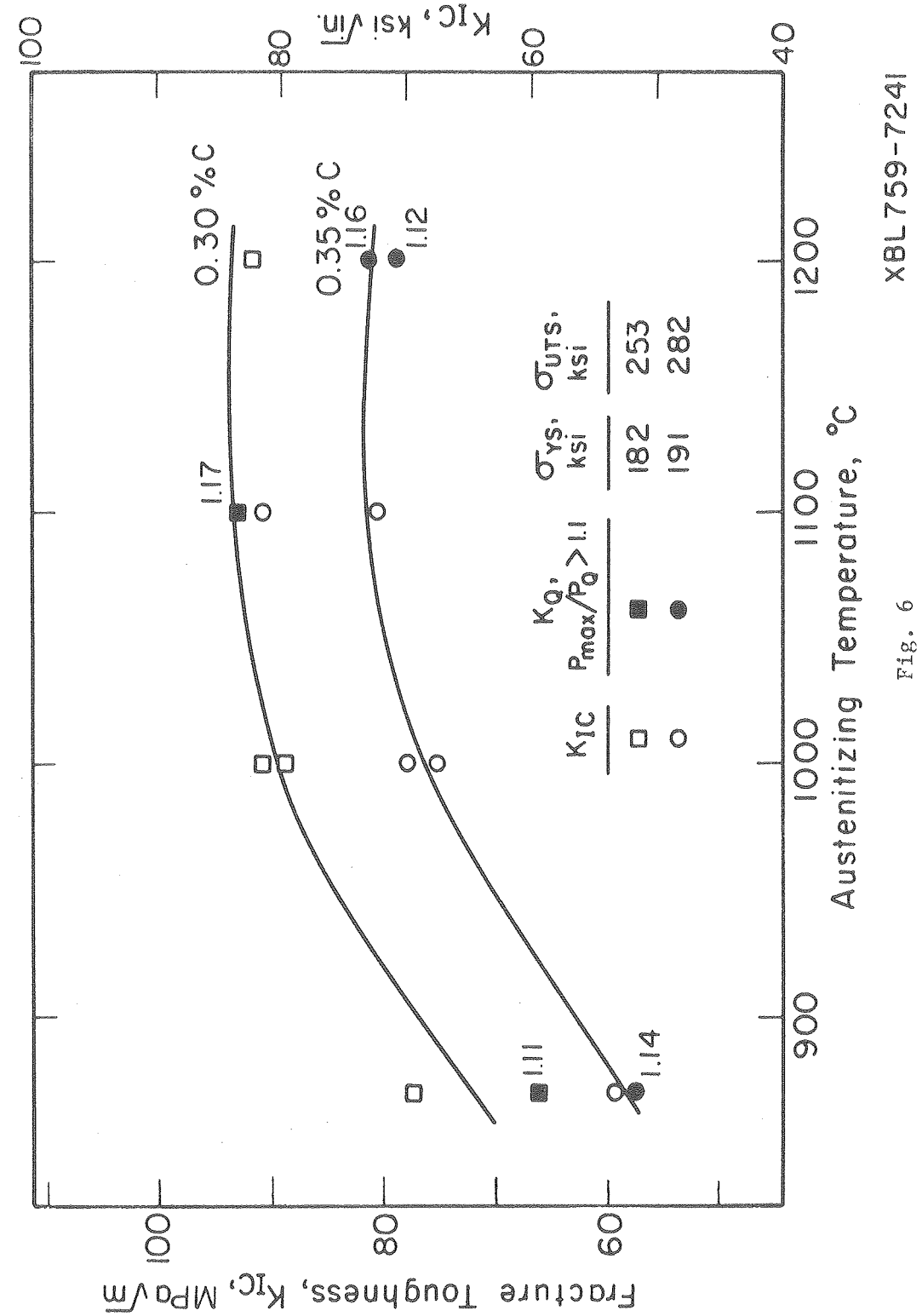
Fracture Toughness, K_{IC}, MPa$\sqrt{m}$
K_{IC}, ksi$\sqrt{in}$
Austenitizing Temperature, °C
0.30 %C
0.35 %C
1.17
1.16
1.12
1.11
1.14
K_{IC}
K_Q, $P_{max}/P_Q > 1.1$
σ_{YS}, ksi
σ_{UTS}, ksi
182
253
191
282
XBL759-7241

Fig. 6

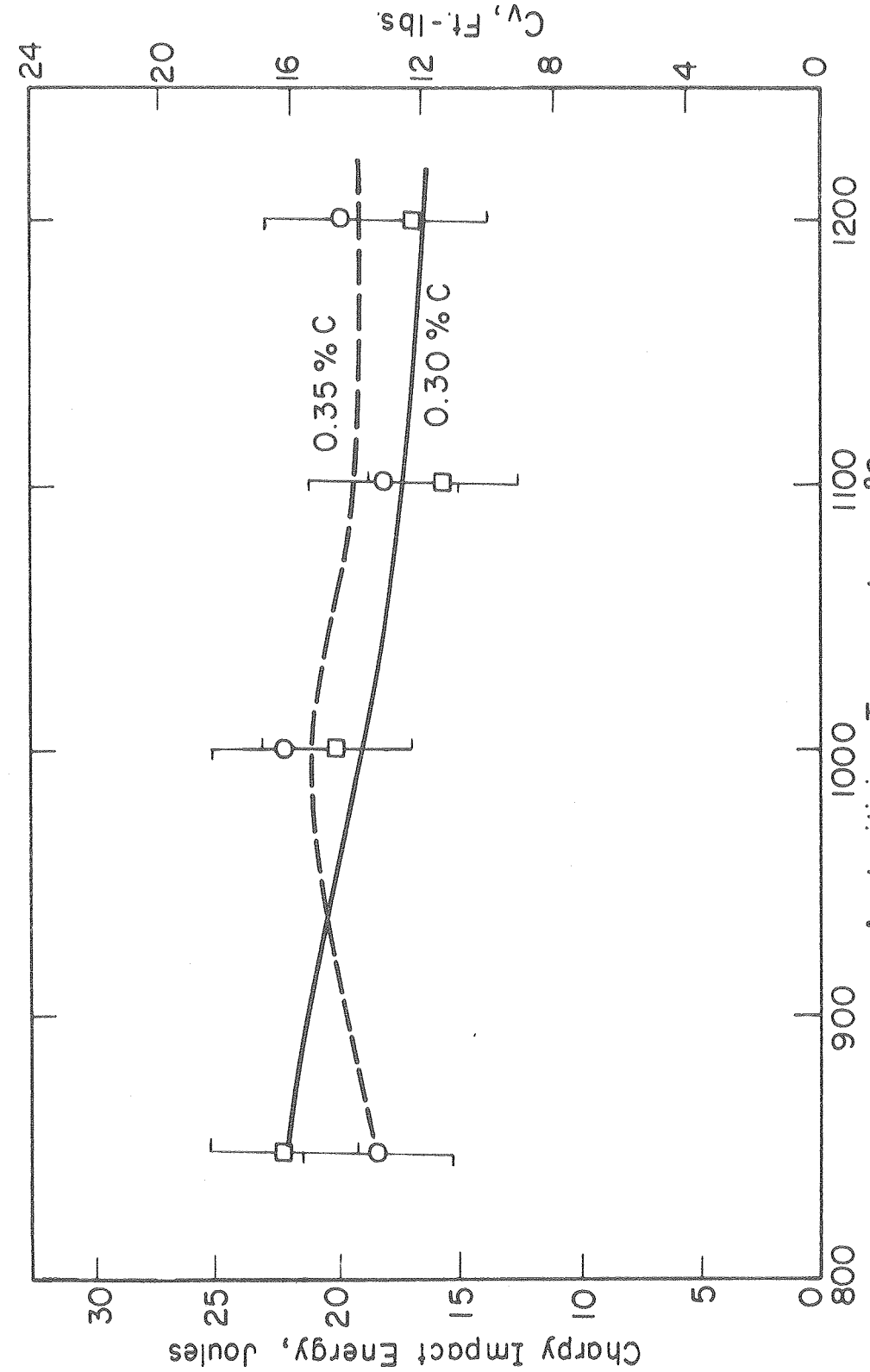

XBL 769-7501

Fig. 7

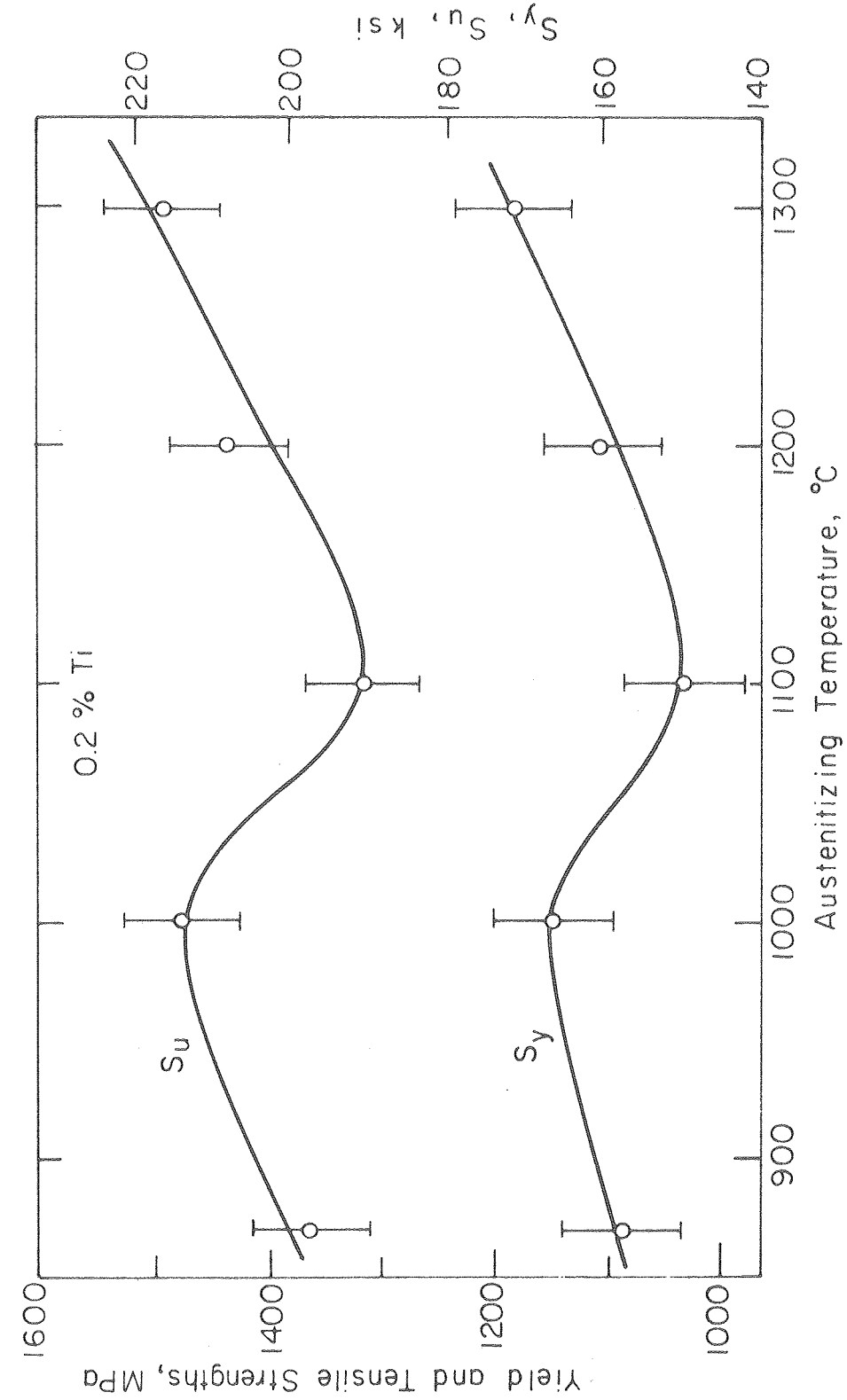

XBL782-4601

Fig. 8

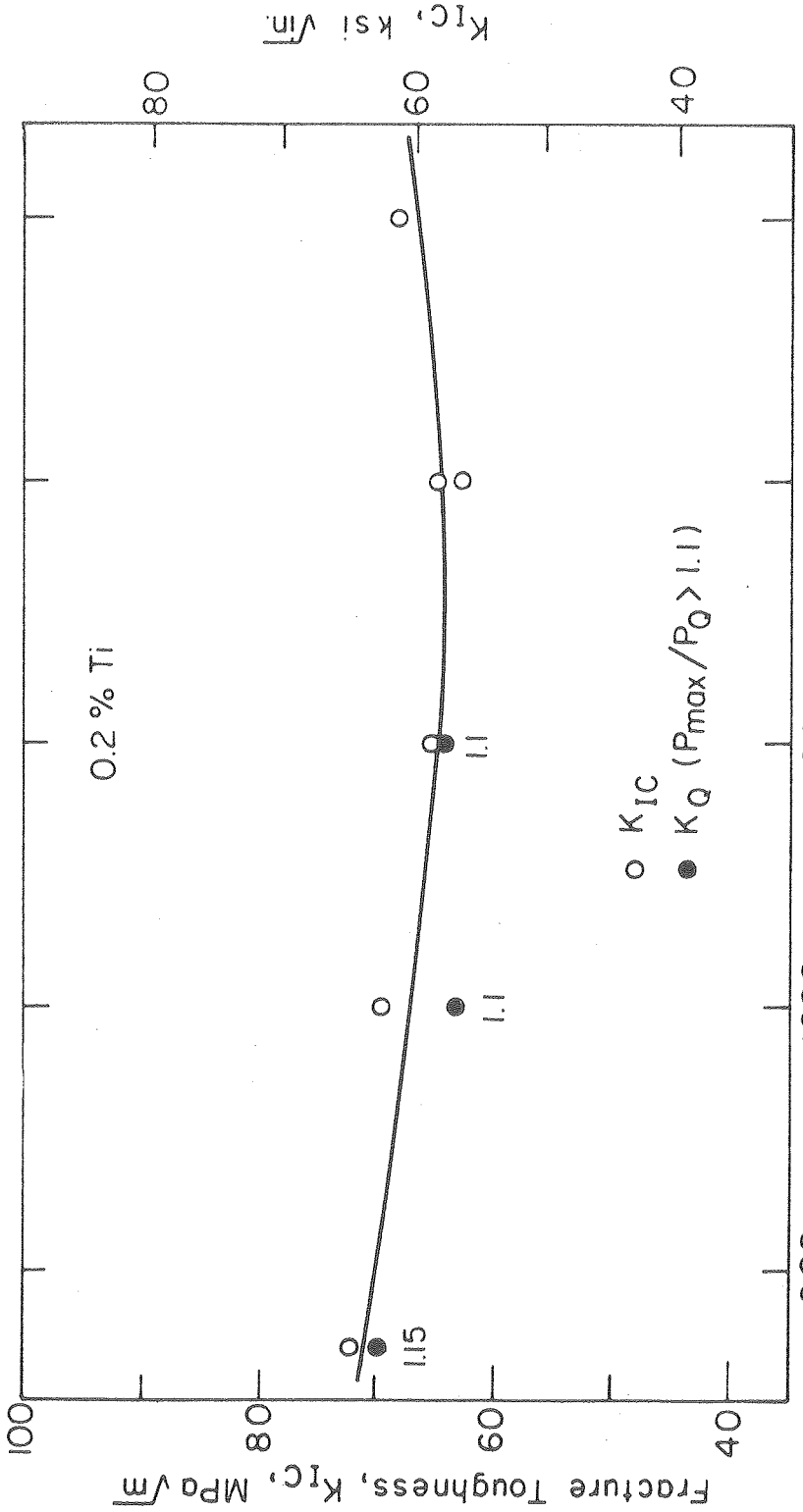

XBL782-4602

Fig. 9

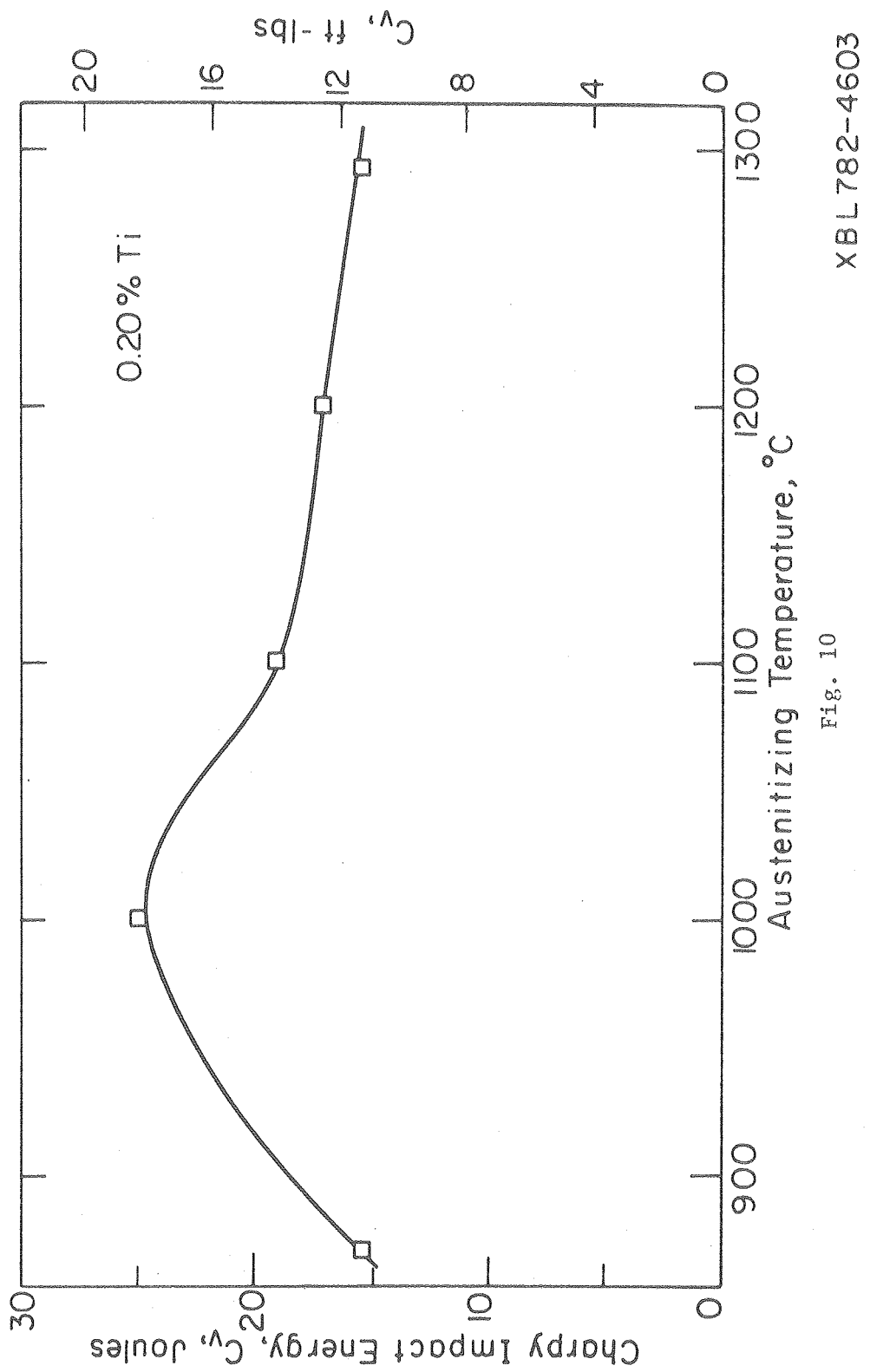

XBL 782-4603

Fig. 10

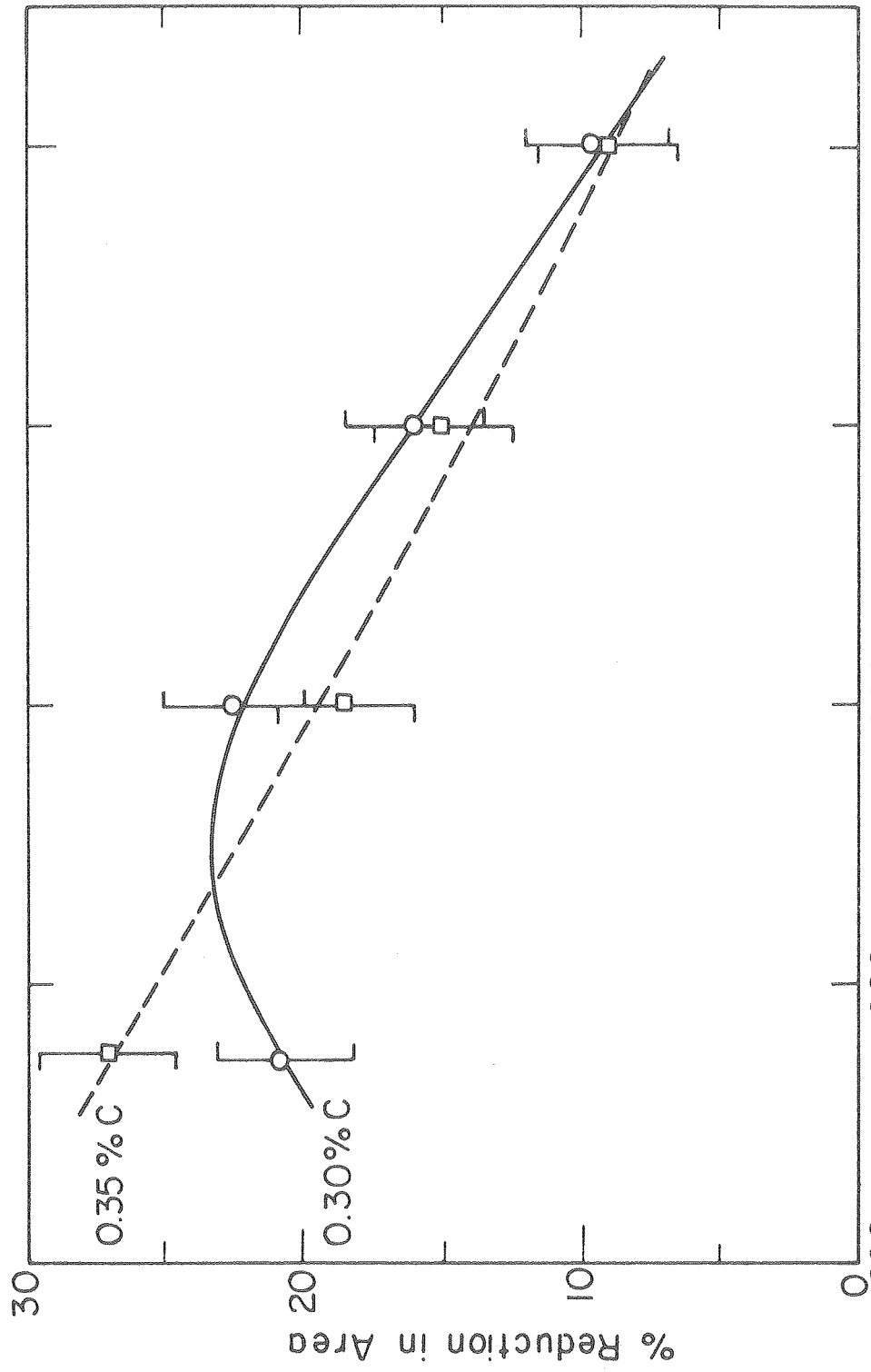
% Reduction in Area
30
20
10
0
800
900
1000
1100
1200
Austenitizing Temperature, °C
0.35 % C
0.30 % C
XBL 762-6514

Fig. 11

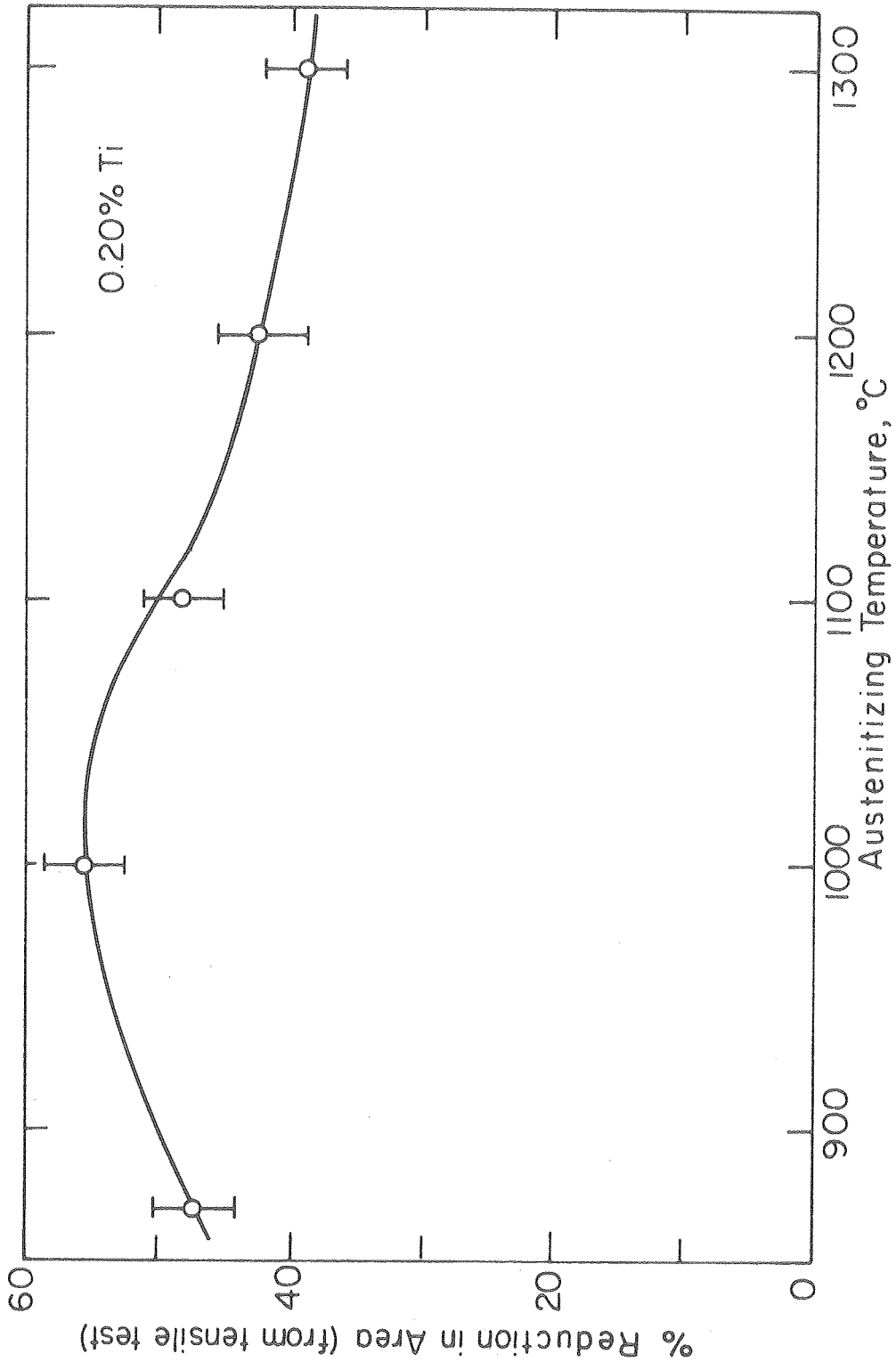
0.20% Ti
% Reduction in Area (from tensile test)
0
20
40
60
900
1000
1100
1200
1300
Austenitizing Temperature, °C
XBL 782-4606

Fig. 12

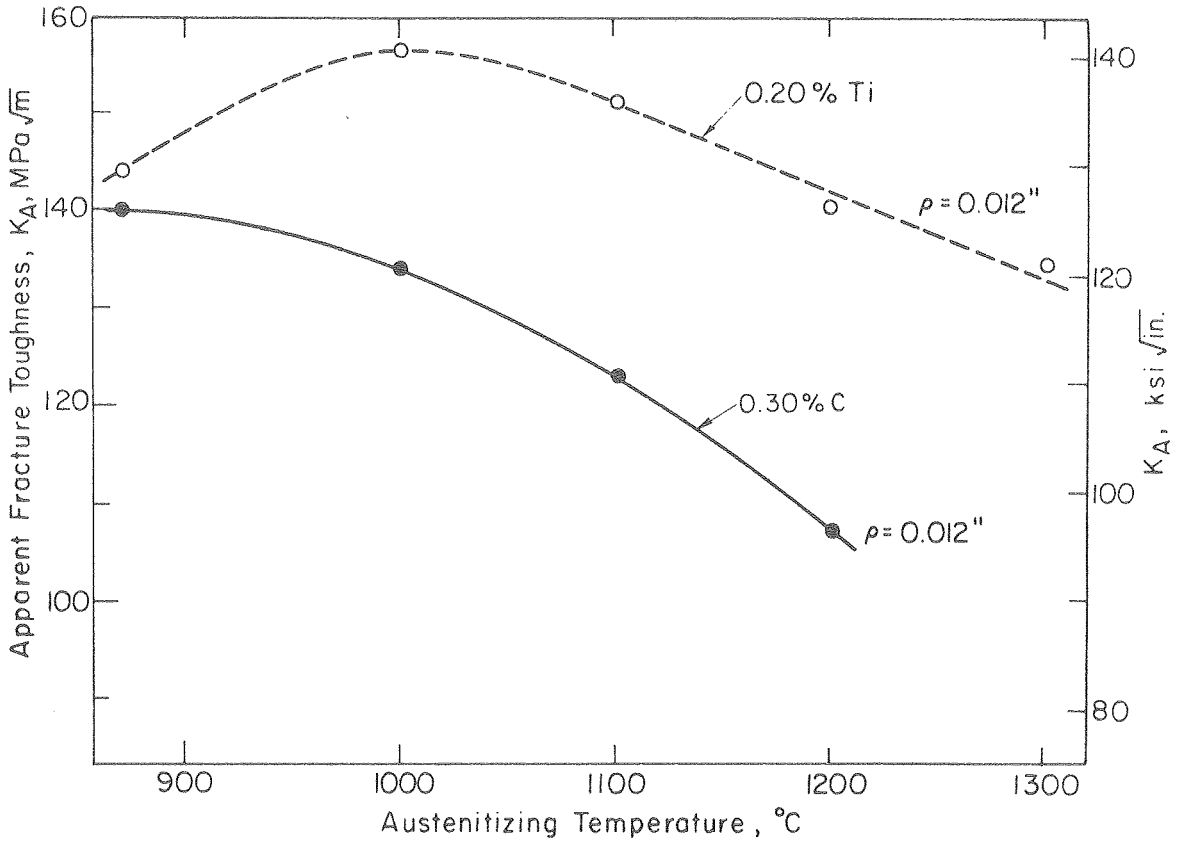
160
140
120
100
Apparent Fracture Toughness, K_A, MPa $\sqrt{m}$
140
120
100
80
K_A, ksi $\sqrt{in.}$
0.20 % Ti
ρ = 0.012"
0.30 % C
ρ = 0.012"
900
1000
1100
1200
1300
Austenitizing Temperature, °C
XBL 782-4604A

Fig. 13

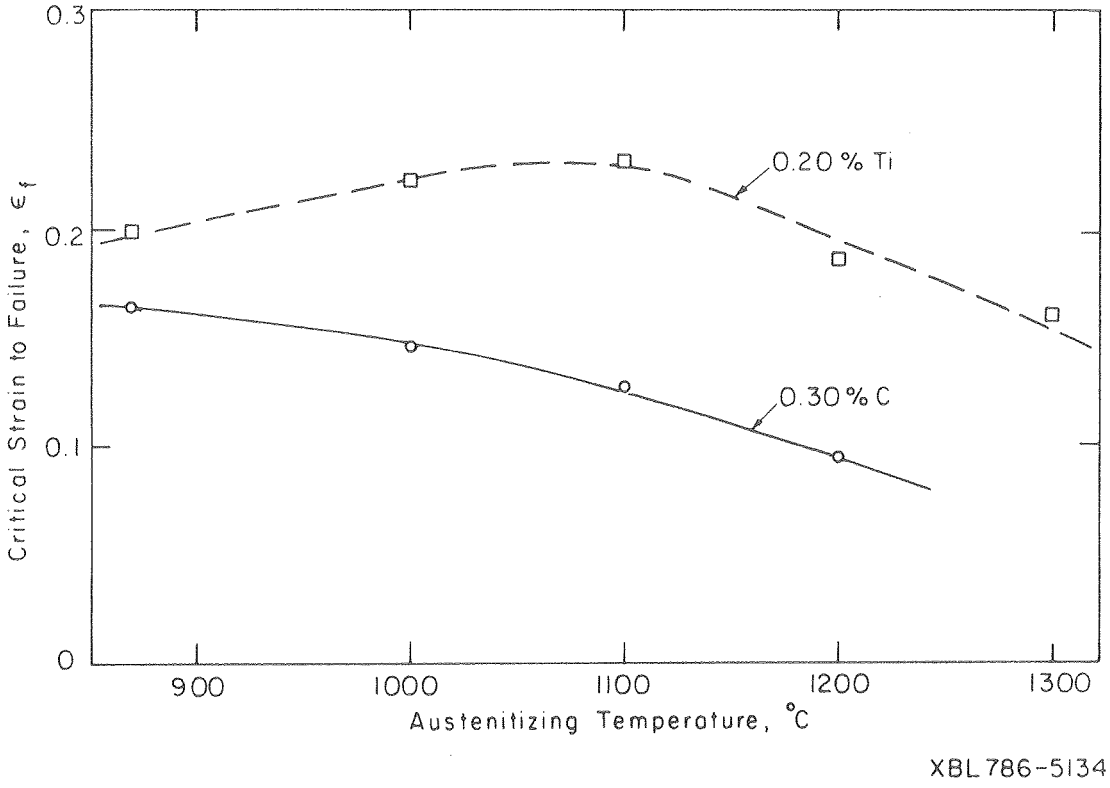
0.3
0.2
0.1
0
Critical Strain to Failure, ϵ_f
0.20 % Ti
0.30 % C
900
1000
1100
1200
1300
Austenitizing Temperature, °C
XBL 786-5134

Fig. 14

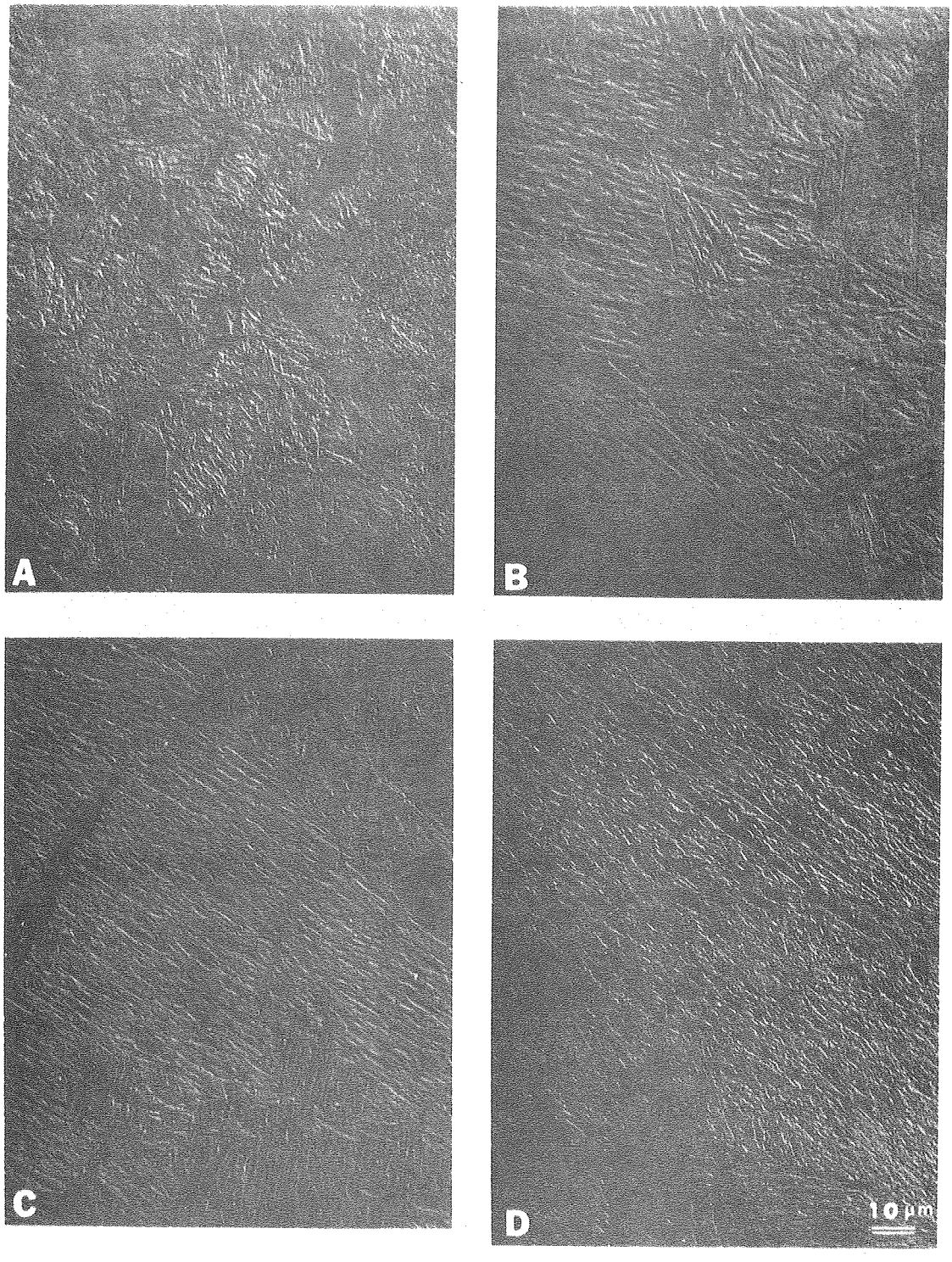

XBB 785-5976

Fig. 15

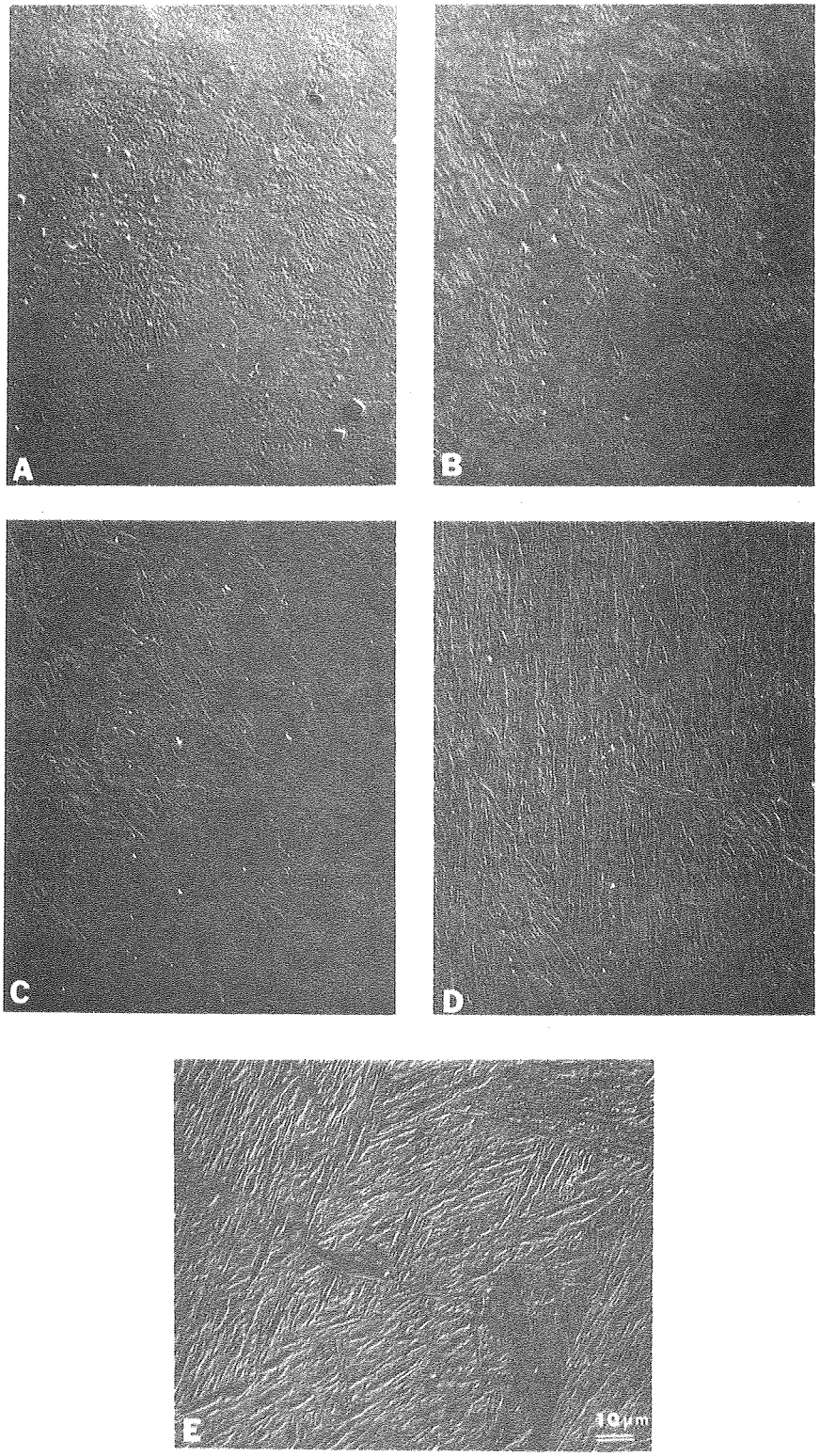

XBB 785-5980

Fig. 16

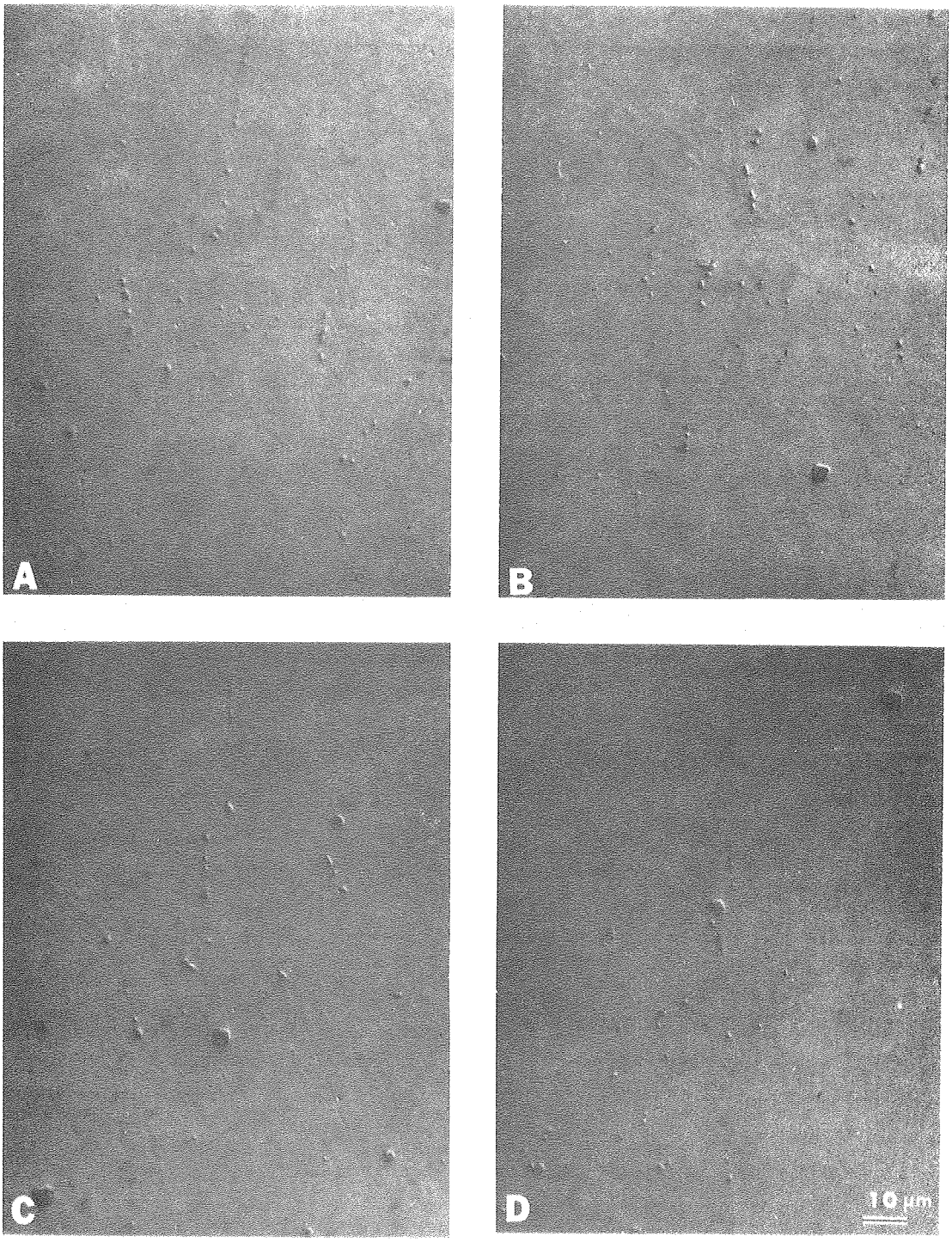

XBB 785-5977

Fig. 17

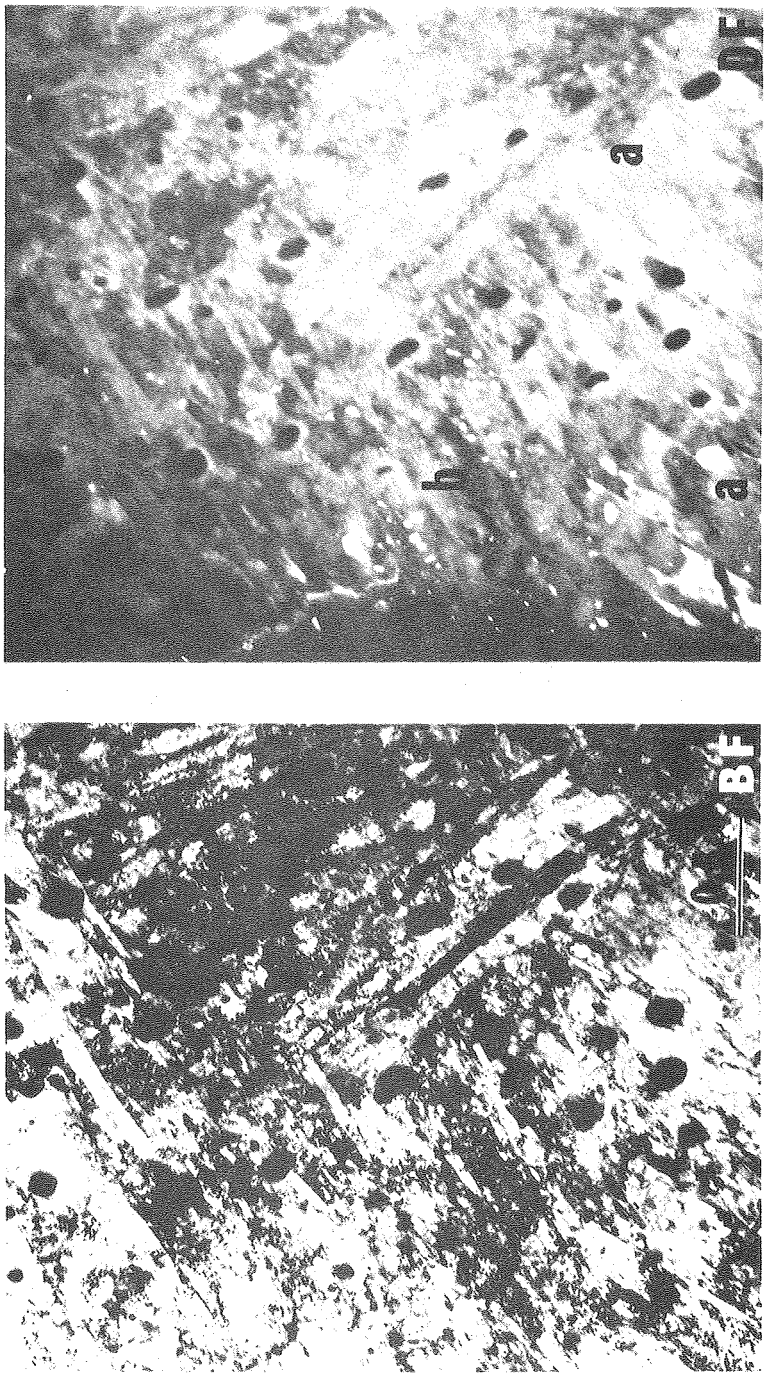

XBB 763-7129

Fig. 18

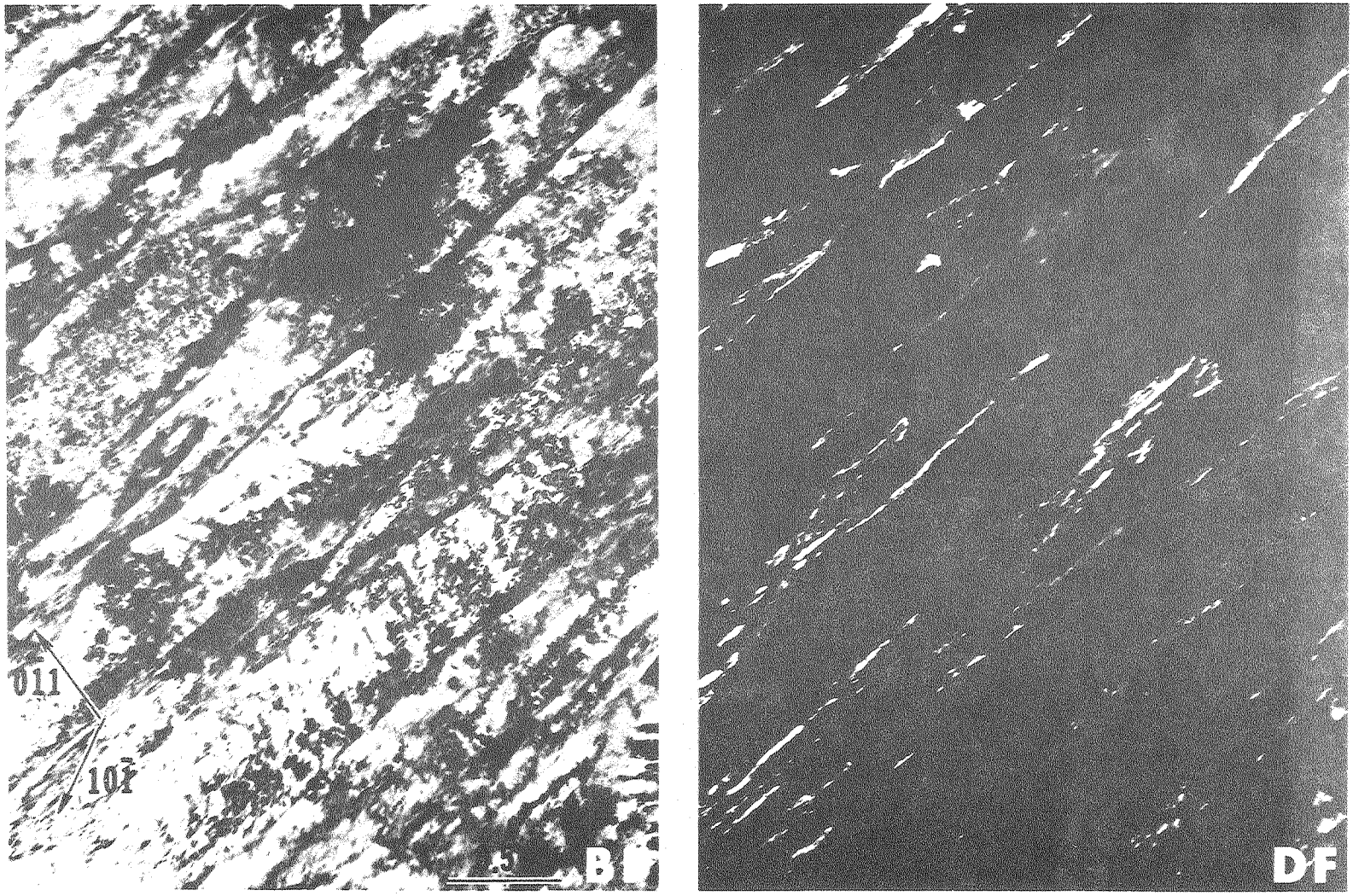

XBB 785-4569

Fig. 19

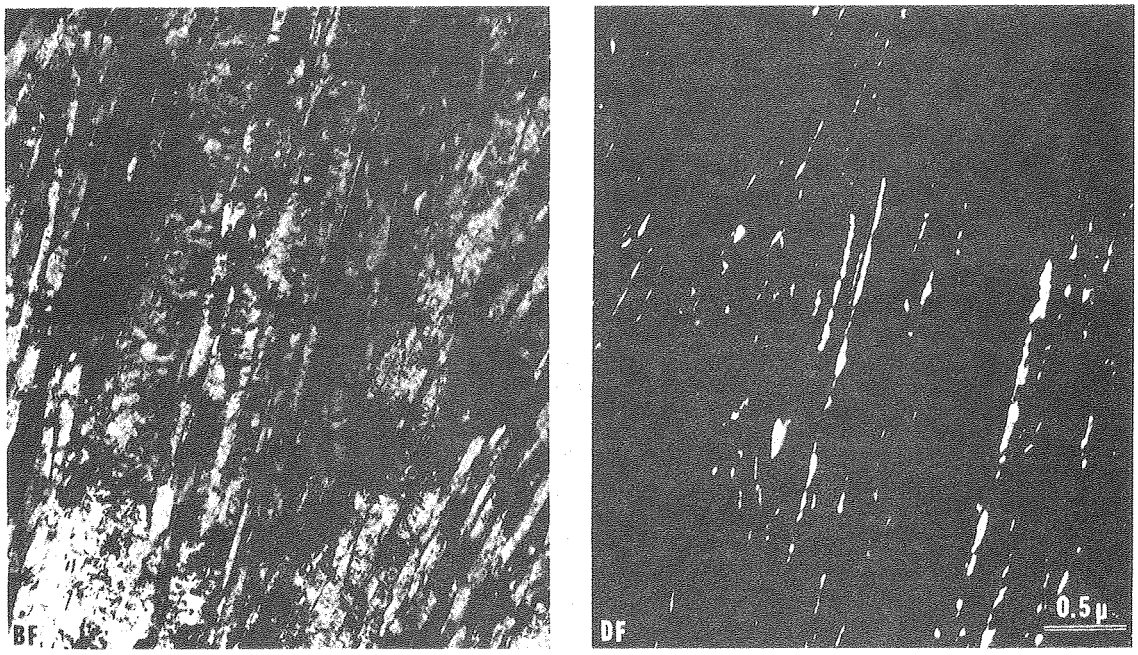

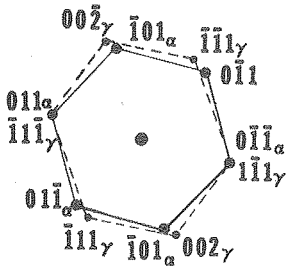

—[111] Martensite Orientation

----[110] Austenite Orientation

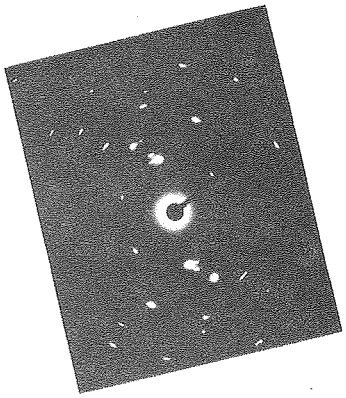

XBB 785-6052

Fig. 20

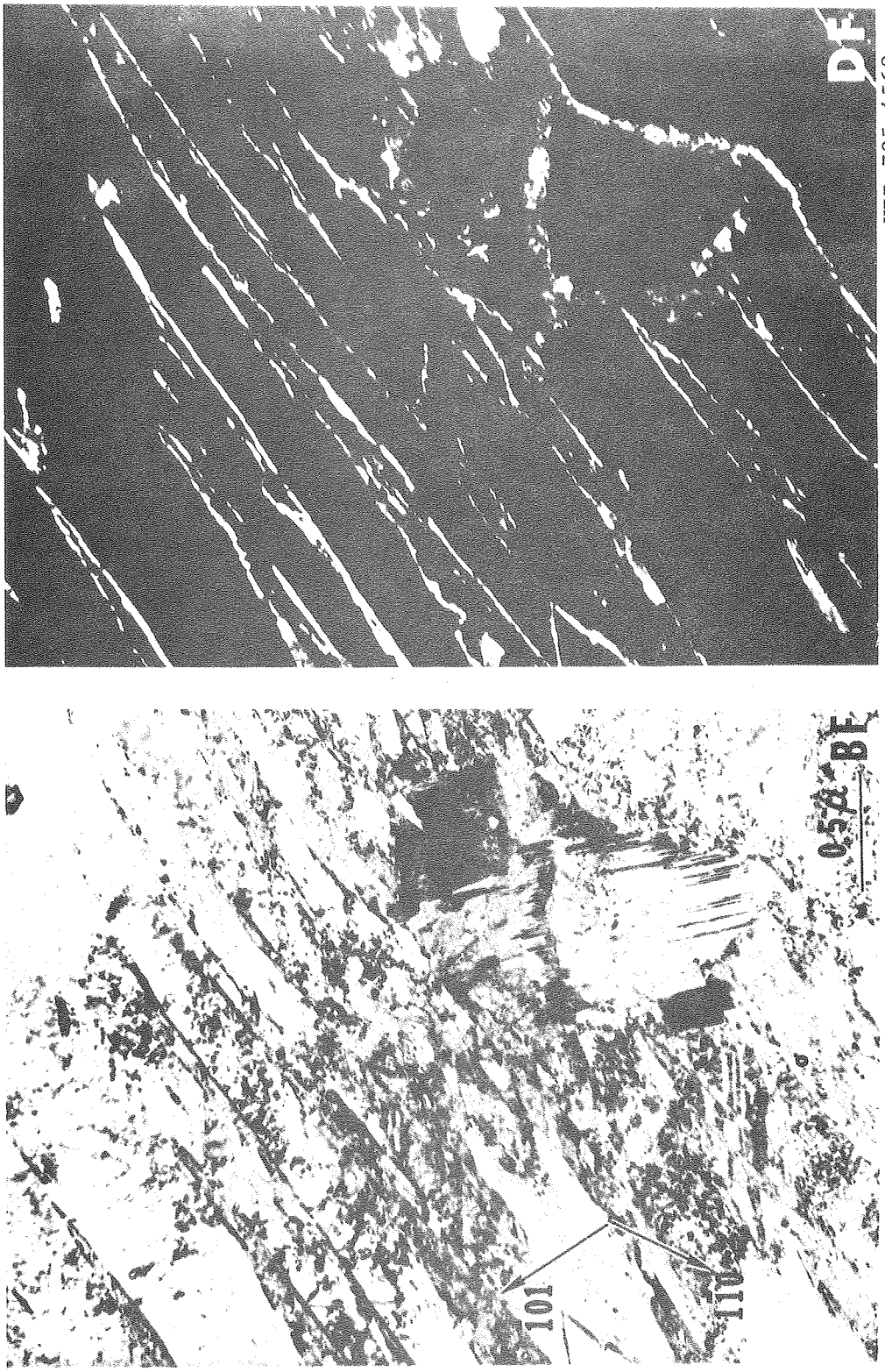

XBB 785-4568

Fig. 21

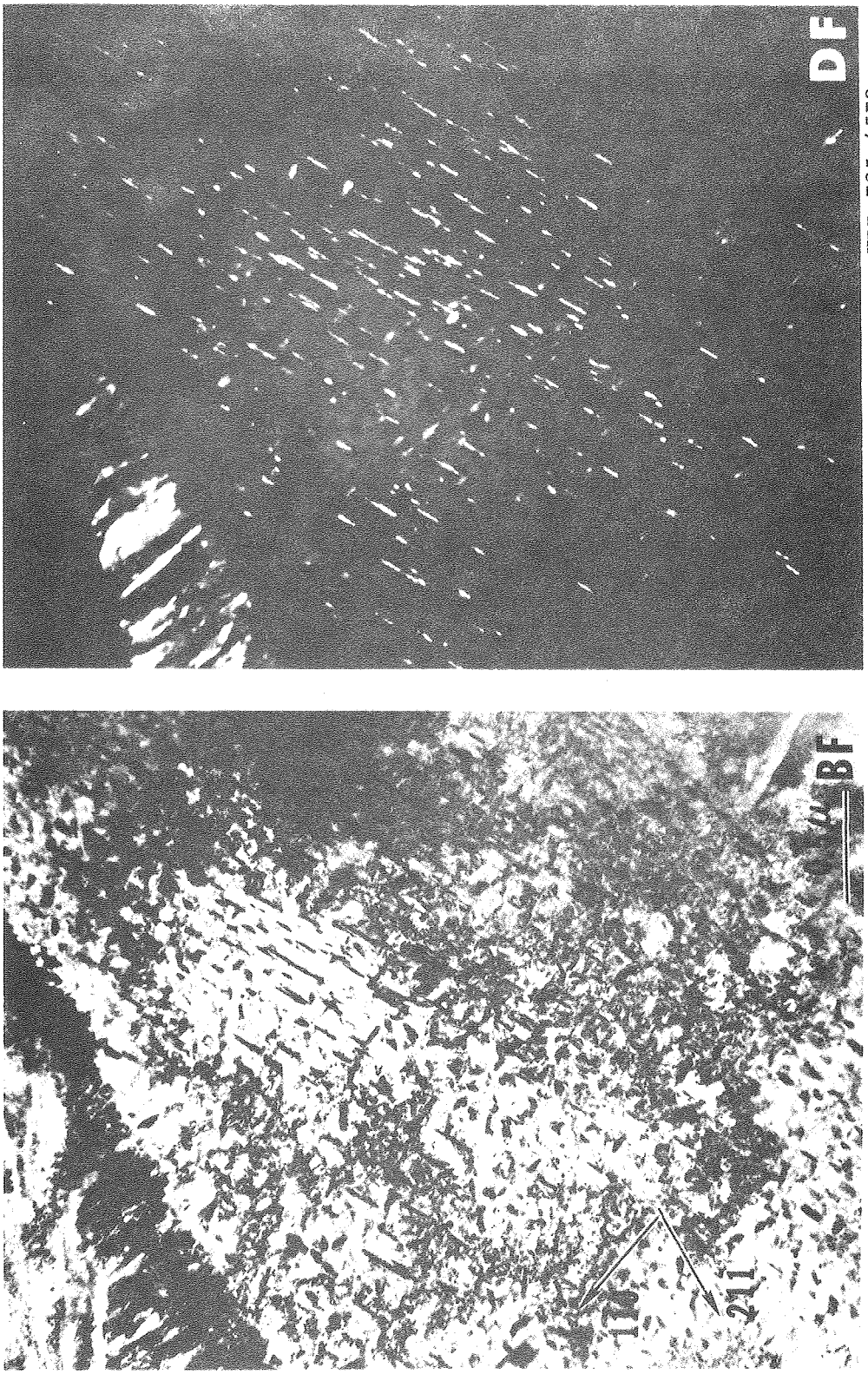

Fig. 22

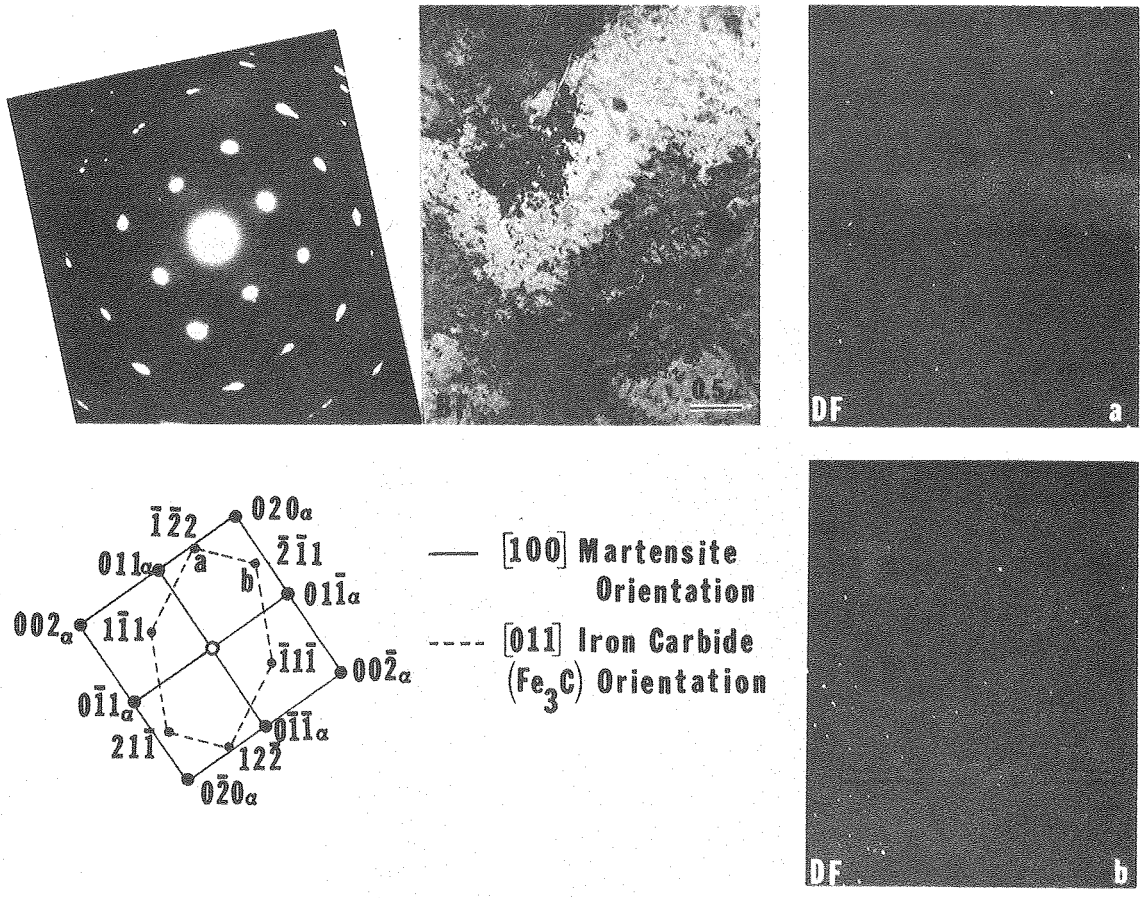
0.5μ
DF
a
DF
b
$\bar{1}\bar{2}2$
020_α
011_α
$\bar{2}\bar{1}1$
$01\bar{1}_\alpha$
002_α
$1\bar{1}1$
$\bar{1}1\bar{1}$
$00\bar{2}_\alpha$
$0\bar{1}1_\alpha$
$0\bar{1}\bar{1}_\alpha$
$21\bar{1}$
$12\bar{2}$
$0\bar{2}0_\alpha$
[100] Martensite Orientation
[011] Iron Carbide (Fe_3C) Orientation
XBB 785-6051

Fig. 23

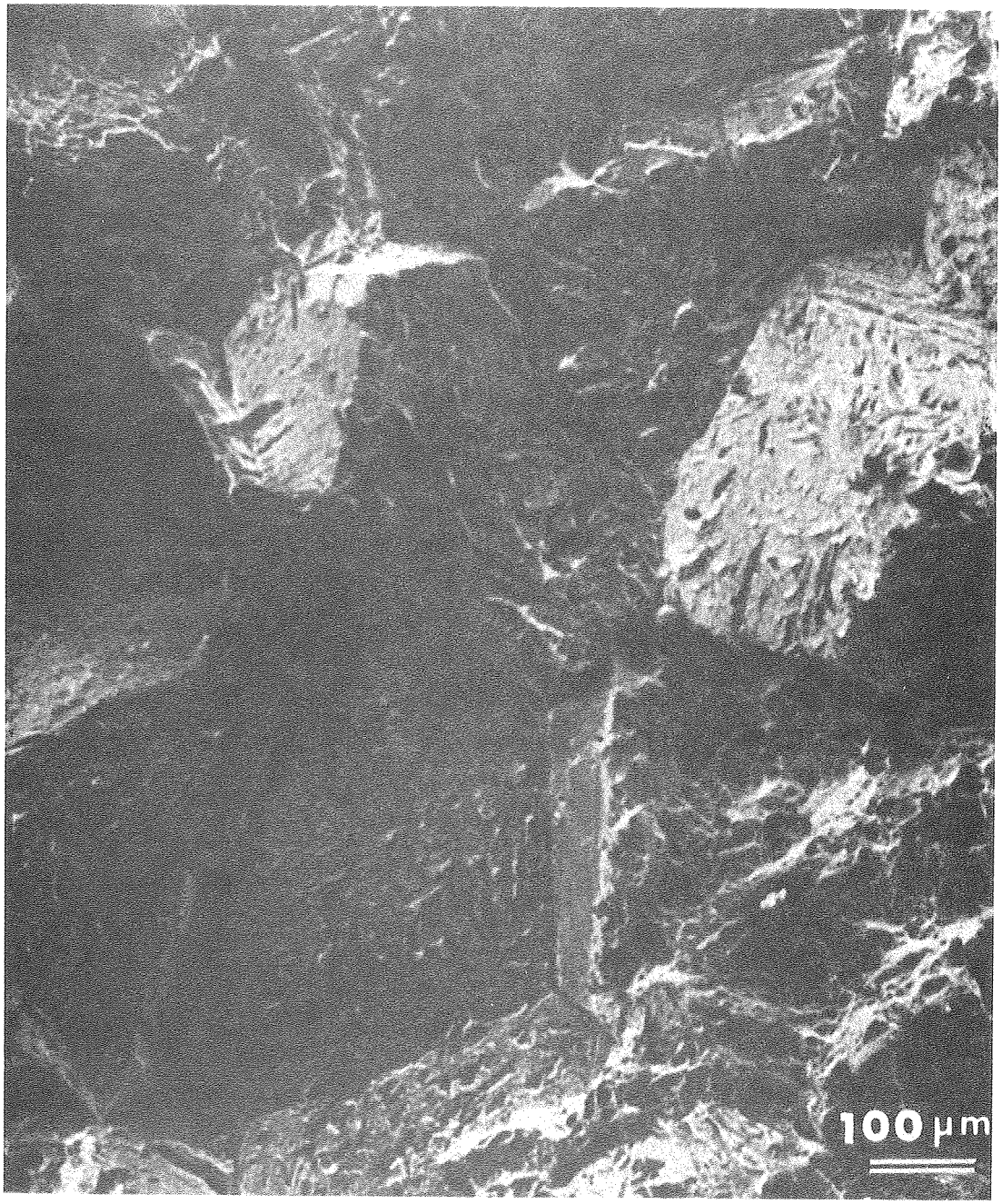

XBB 785-5975

Fig. 26

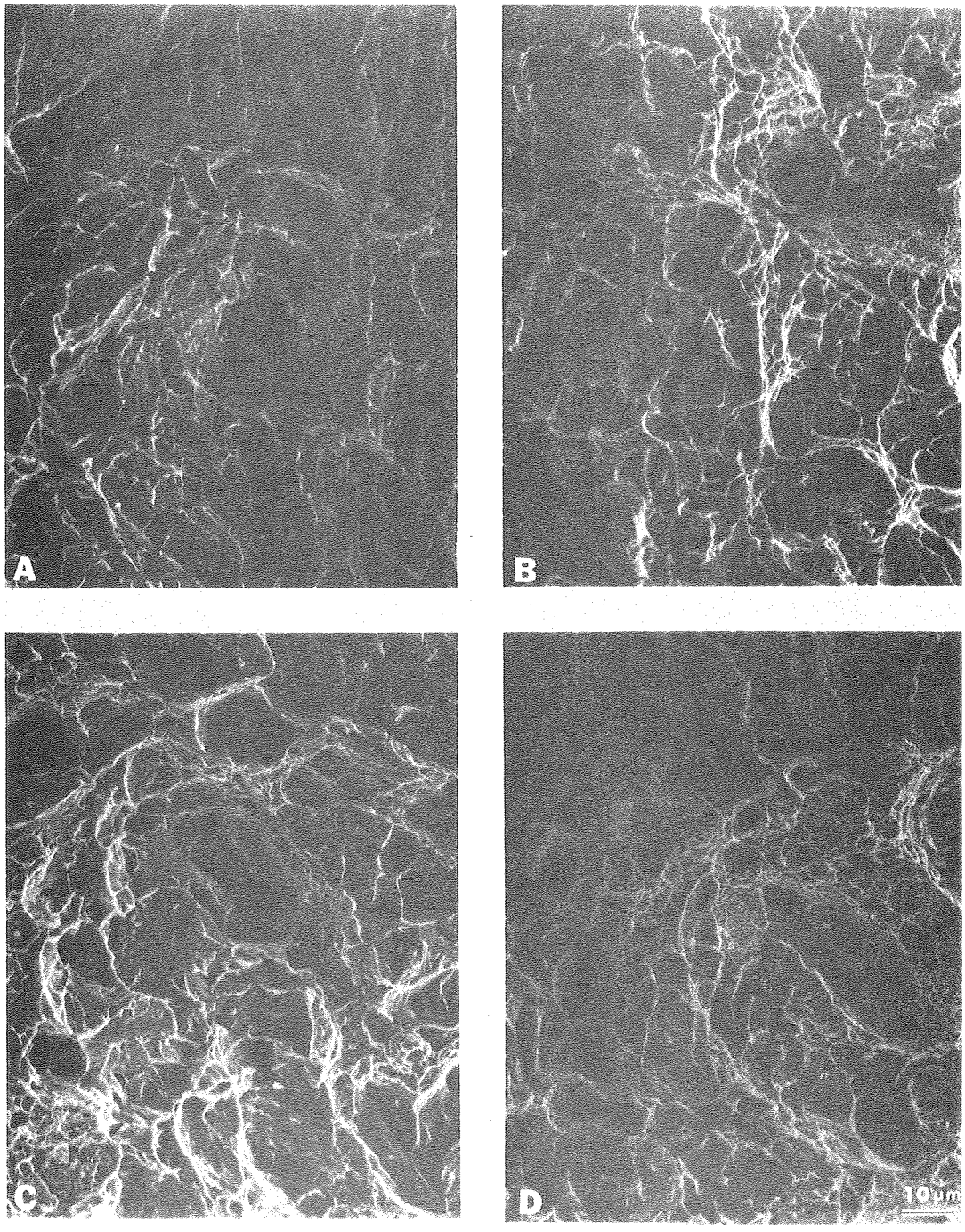

XBB 785-5979

Fig. 27

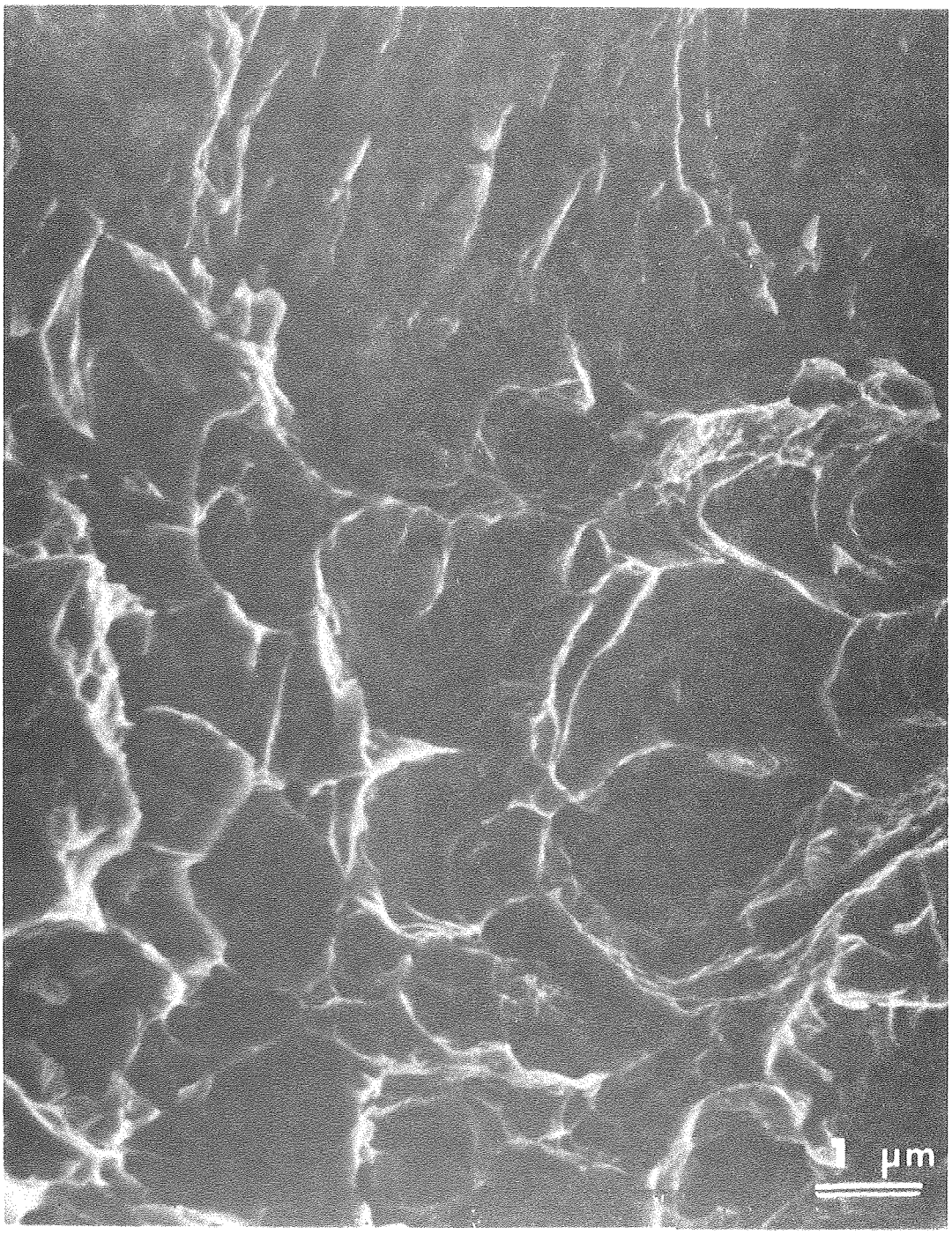

XBB 785-5974

Fig. 28

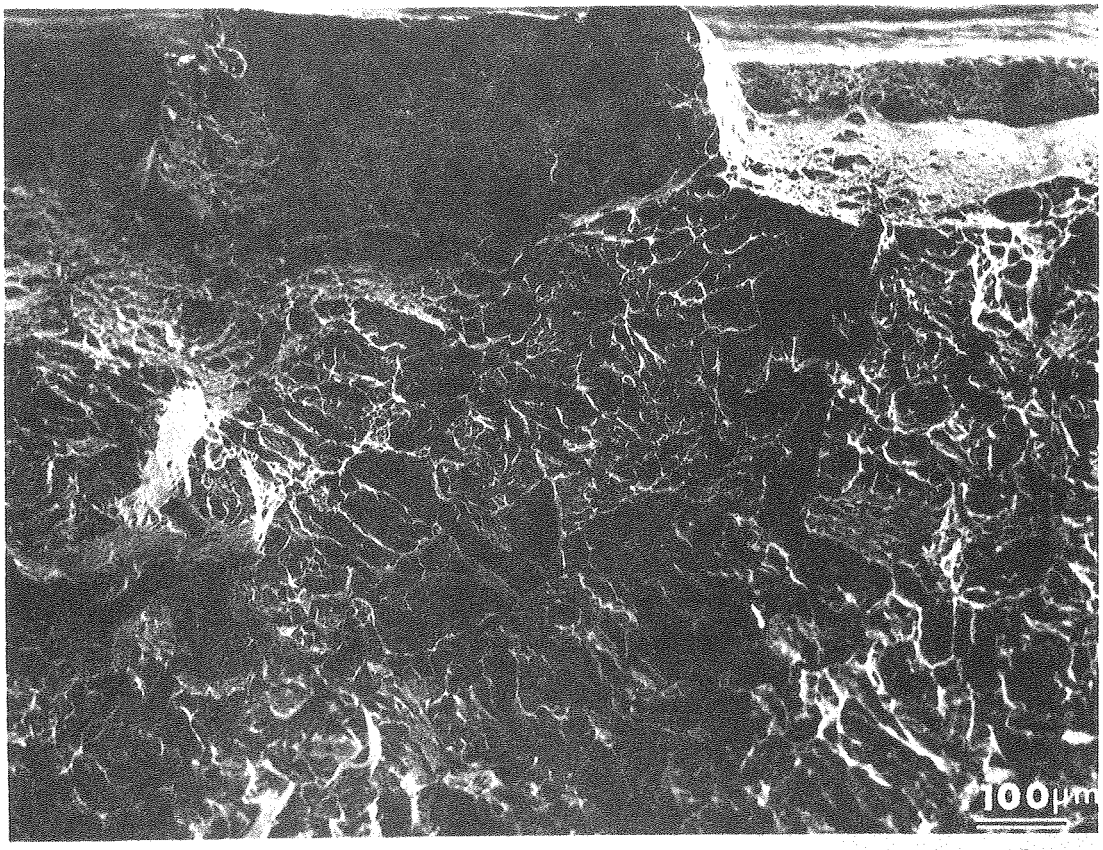

XBB 785-5981

Fig. 29